Photocatalysis with MOFs

International Edition: DOI: 10.1002/anie.201505581
German Edition: DOI: 10.1002/ange.201505581

Metal–Organic Framework (MOF) Compounds: Photocatalysts for Redox Reactions and Solar Fuel Production

Amarajothi Dhakshinamoorthy, Abdullah M. Asiri, and Hermenegildo García**

Keywords:
CO_2 reduction · H_2 generation · metal–organic frameworks · photocatalysis · solar fuels

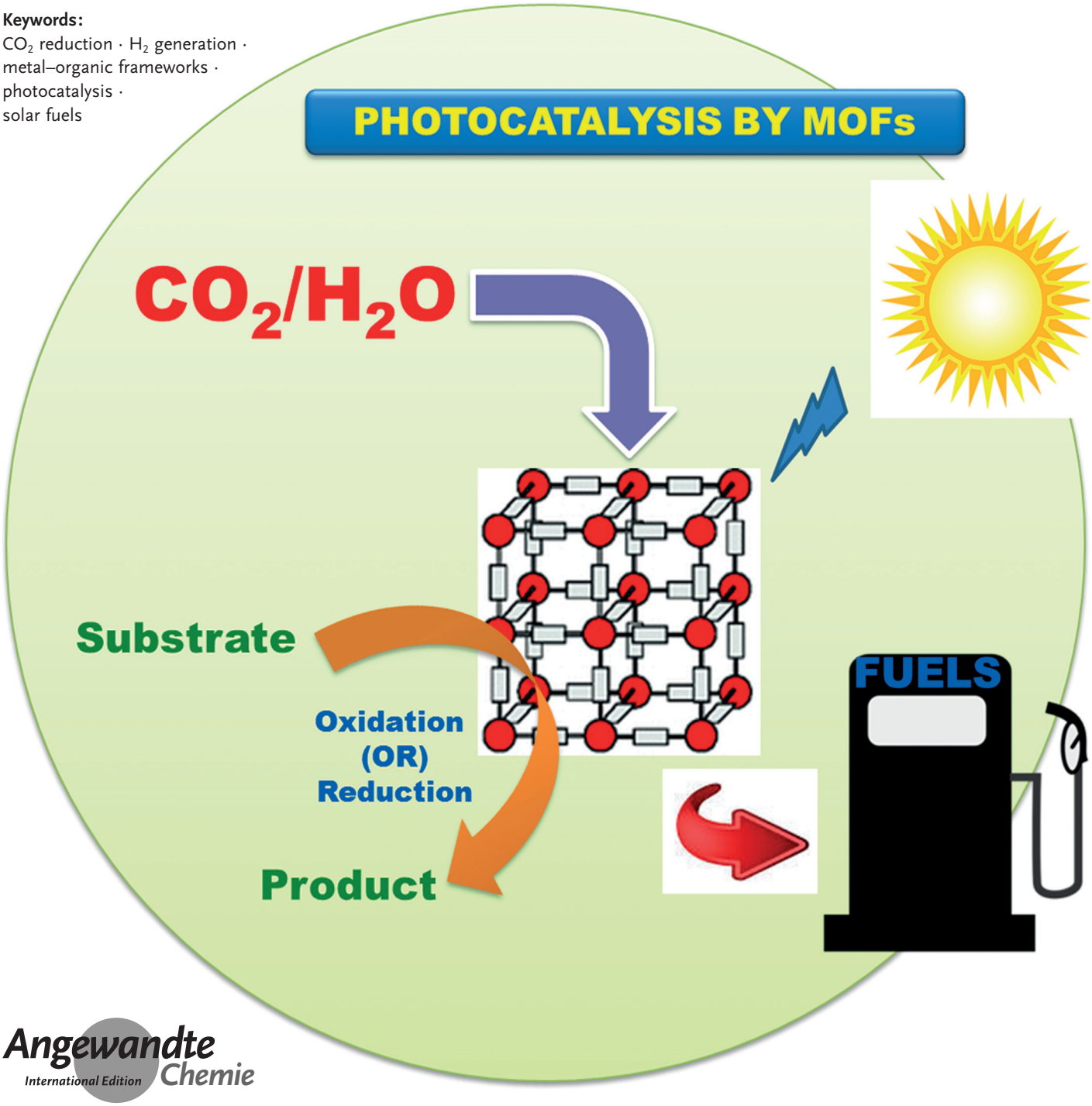

Metal–organic frameworks (MOFs) are crystalline porous materials formed from bi- or multipodal organic linkers and transition-metal nodes. Some MOFs have high structural stability, combined with large flexibility in design and post-synthetic modification. MOFs can be photoresponsive through light absorption by the organic linker or the metal oxide nodes. Photoexcitation of the light absorbing units in MOFs often generates a ligand-to-metal charge-separation state that can result in photocatalytic activity. In this Review we discuss the advantages and uniqueness that MOFs offer in photocatalysis. We present the best practices to determine photocatalytic activity in MOFs and for the deposition of co-catalysts. In particular we give examples showing the photocatalytic activity of MOFs in H_2 evolution, CO_2 reduction, photooxygenation, and photoreduction.

From the Contents

1. Introduction and Historical Perspective

Organic photochemistry started to develop in the 1960s and became a mature science in the 1980s, achieving a remarkable degree of understanding of the processes triggered upon light absorption.[1] The progress in transient absorption spectroscopy and various fast spectroscopic techniques with the use of short (ns) and ultra-short (fs or ps) pulsed lasers made possible the detection of electronic singlet and excited states of organic chromophores as well as reaction intermediates generated as a consequence of light absorption.[2] Kinetic measurements in the presence of quenchers allowed the determination of the reactivity of these transient species in processes such as energy or electron transfer.[1]

Initial photochemical studies were carried out in solution. However, as photochemistry progressed and aimed at gaining control on the photochemical reactivity, it soon became apparent that the use of surfaces and confined spaces is a powerful methodology to achieve selectivity towards a desired pathway.[3] Pioneering studies by de Mayo showed that photochemical reactions on the solid surfaces of silica give a different product distribution in radical coupling than in solution.[4] The general outcome is that adsorption on solid surfaces favors reaction pathways arising from restricted mobility, such as geminate radical recombination in the case of carbon centered radicals or photodimerization.[5]

From these seminal studies of 2D photochemistry, researchers were, subsequently, interested in the use of porous materials which offer the confinement of intermediates in 3D.[6] Porosity allows mass transfer from the exterior to the interior of a solid particle, where the reaction can take place inside a rigid reaction cavity with nanometric dimensions and having specific properties in terms of polarity and the presence of acids or redox sites. Porous solids allows confinement of the photochemical reaction to a restricted space, with the porous material acting as a rigid matrix.[3]

Zeolites were among the preferred porous materials for these photochemical studies in heterogeneous media, owing to their large porosity and large surface area.[7] Figure 1 presents some of the general topologies for zeolites.[7] The aluminosilicate composition of zeolites allows the light to penetrate a few microns into films of opaque zeolite powders reaching chromophores inside their pores. Photochemical reactions could also take place by suspending the solids in a liquid phase to allow a better exposure of the material to photons.[8]

However, zeolites mostly play a passive role, since they cannot undergo direct photoexcitation. Several effects were observed as a consequence of the immobilization of the

[*] Prof. Dr. A. Dhakshinamoorthy
School of Chemistry, Madurai Kamaraj University
Madurai-21, Tamil Nadu (India)
E-mail: admguru@gmail.com
Prof. Dr. A. M. Asiri, Prof. Dr. H. García
Centre of Excellence for Advanced Materials Research
King Abdulaziz University, Jeddah (Saudi Arabia)
Prof. Dr. H. García
Instituto de Tecnología Química, CSIV-UPV
Av. De los Naranjos s/n, 46022, Valencia (Spain)
E-mail: hgarcia@qim.upv.es
ORCID(s) from the author(s) for this article is/are available on the WWW under http://dx.doi.org/10.1002/anie.201505581.

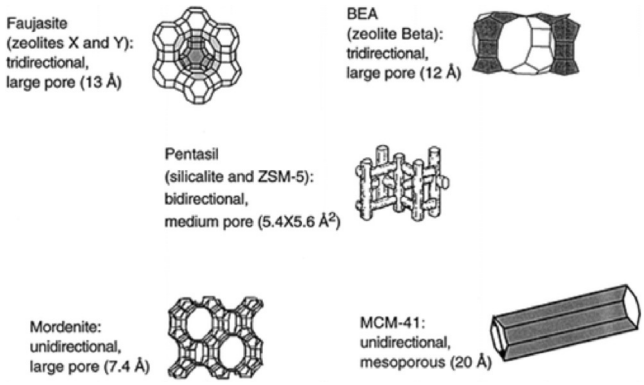

Figure 1. Voids and topologies of some common zeolites and porous aluminosilicate (reproduced with permission from Ref. [7]).

organic substrate (Scheme 1).[9] The polarity of the internal voids of zeolites[10] in the presence of alkali-metal ions and negative oxygen atoms can be so high (21 V nm^{-1} in the case of Li^+-exchanged Y) that it favors photoinduced electron transfer between photoexcited guests and incorporated electron-donor or electron-acceptor molecules.[10,11] Given the structural similarities between zeolites and MOFs that are the subject of this Review, photocatalysis in MOFs can be considered as the logical evolution of the initial studies in zeolites.

In parallel to organic photochemistry, another field that was developing intensively since the late 1970s was photocatalysis, mainly based on the activity of semiconducting TiO_2

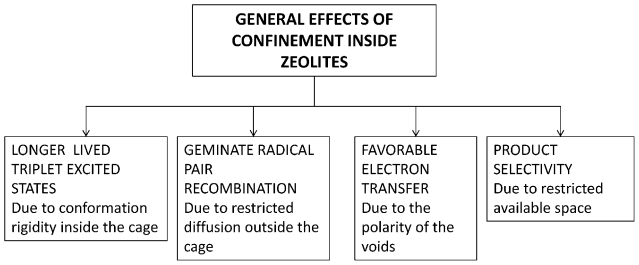

Scheme 1. General effects observed in the photochemistry of incorporated guest molecules as a consequence of performing the reaction inside the pores of zeolites.

in the anatase form.[11,12] The field of photocatalysis was focused initially in the degradation of organic pollutants in low concentrations in H_2O or in air.[11] Upon irradiation in the UV, TiO_2 reaches a state of charge separation and a fraction of electrons and positive holes can reach the external surface of the particle and react with substrates adsorbed on the surface of TiO_2 nanoparticles. The hallmark features of a semiconductor are the generation of the charge-separate state upon irradiation with photons of energy larger than the bandgap of the material and the mobility of the charge carriers that migrate away from the site at which the charge separation event has taken place (Scheme 2).[12] It will be

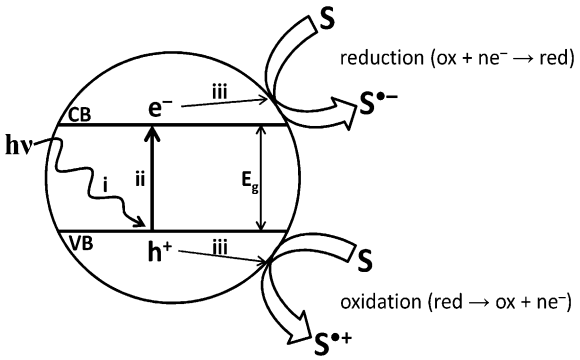

Scheme 2. Elementary steps occurring in a photocatalytic event: i) light absorption, ii) electron promotion from the valence band (VB) to the conduction band (CB), iii) charge migration to the surface of the particle, oxidation of substrate (S) by the positive hole (h^+), reduction of S by electron (e^-).

commented later that charge mobility is a requirement that is generally not fulfilled in the photochemistry of MOFs.[13]

The constant target in this area has been to increase the efficiency of the photocatalytic process and one of the limitations was the lack of photo response of wide bandgap semiconductors to visible light or their unsatisfactory activity under solar-light exposure.[13,14] Thus, there is a need to develop photocatalysts with visible-light activity.

One of the most successful strategies to achieve this goal is employed in dye-sensitized solar cells and consists in using an organic chromophore for light harvesting that after excitation

Amarajothi Dhakshinamoorthy received his PhD from Madurai Kamaraj University in 2009 and was a postdoctoral researcher at the Technical University of Valencia with Prof. Hermenegildo Garcia. Since June 2013, he is UGC-Assistant Professor at the School of Chemistry, Madurai Kamaraj University. His research interests include the application of metal–organic frameworks and graphene-related materials in heterogeneous catalysis. He is the recipient of the Young Scientist Award 2014 for Chemical Sciences from The Academy of Sciences, India.

Abdullah M. Asiri received PhD from University of Wales, College of Cardiff, UK, in 1995. Since 2009 he has been the Head of the Chemistry Department at King Abdulaziz University and he is the founder and the Director of the Center of Excellence for Advanced Materials Research. He is a Professor of Organic Photochemistry. His research interest covers color chemistry, photochromic and thermochromic systems, dyes, nanotechnology and polymers. He is the Vice-President of Saudi Chemical Society (Western Province Branch).

injects one electron to the semiconductor conduction band (CB).[14,15] In a certain way, dye sensitization of TiO_2 and other inorganic semiconductors is an indirect methodology to produce a visible-light photoresponse in inorganic materials that has been extremely successful for the preparation of dye-sensitized solar cells in comparison with the development of visible-light-absorbing inorganic photocatalysts (Figure 2).[16–18]

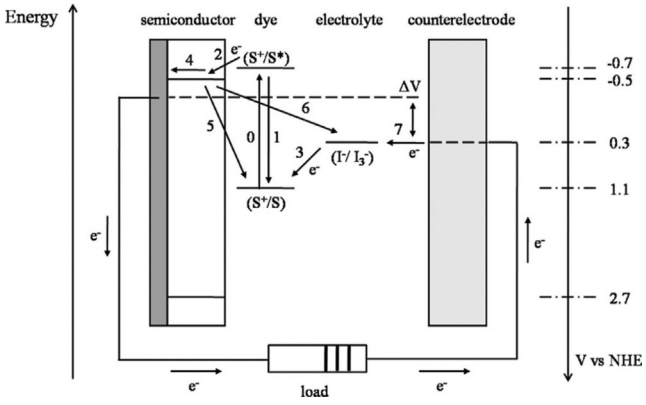

Figure 2. Operation diagram of a dye-sensitized solar cell with some indication of the energy levels (corresponding to N3 dye, TiO_2, and a redox couple). The paths followed by electrons are indicated by the numbers 1–7 (0: photoexcitation, 1: relaxation, 2: injection from excited dye to the semiconductor conduction band, 3: annihilation of the electron hole by the redox couple in the electrolyte, 4: migration of electrons to the electrode, 5: charge recombination from the semiconductor to the oxidized form of the dye, 6: charge recombination from the semiconductor to the oxidized form of the electrolyte, and 7: reduction of the redox couple of the electrolyte by electrons in the cathode. (Reproduced with permission from Ref. [14].)

Another recurrent theme in photocatalysis has been the influence of the material particle size on the photocatalytic activity and, specifically, the operation of "quantum size effects" when the particle size was commensurate with the mobility of the charge carriers.[19,20] Quantum dots, mainly sulfides and chalcogenides of transition metals, exhibit interesting emission and photocatalytic activity as a consequence of their small particle size that confines the exciton in a nanometric particle. In general, quantum confinement shifts light absorption to the visible region as a consequence of the increase in the bandgap energy. This is the case of TiO_2, where small nanometric clusters absorb light at about 300 nm. However, in the case of metal chalcogenides, clusters and small nanoparticles (NPs) about 1 nm are interesting photocatalysts owing to their visible-light absorption.[21] Photocatalysis with semiconductors has experienced a revival in recent years owing to its potential beyond its classical use in pollutant degradation, for the conversion of solar-light energy into chemicals.[22,23]

In view of these precedents, it is not surprising that MOFs also attracted the attention of researchers on photocatalysis and photochemistry as photoresponsive solids with certain similarities to zeolites and metal oxide photocatalysts. As a result of their structure and composition, MOFs combine most of the properties that have been sought, for the development of photoresponsive materials and photocatalysts.

2. MOFs as Photoresponsive Materials

MOFs are crystalline porous materials composed of rigid bi- or multipodal organic linkers and metal ions or clusters of metal ions (Figure 3).[24–26] The metal centers act as nodes of the lattice and are held in place by the directionality of their binding to the organic linkers (electrostatic attraction and coordinative metal–ligand interactions). Crystallinity and porosity are the main characteristics of MOFs and these materials hold records in terms of high pore volume, surface area, and lowest framework density (Figure 4). These properties have determined that one of the main applications of MOFs is as gas adsorbents and for gas separation.[27–29] However, it is also interesting to note that amorphous aminogel $Fe_3O(H_2O)_2F\{C_6H_4(CO_2)_2NH_2\}_3$ which has a similar chemical composition to MIL-100(Fe) $Fe_3O(H_2O)_2F\{C_6H_3(CO_2)_3\}_2$ exhibited notable photocatalytic activity.[30] These data clearly demonstrate that the crystallinity is not an essential requirement for a MOF to show a photocatalytic activity. The reader is also referred to other references for a detailed description of the structure, synthesis, properties, and applications of MOFs.[31–34]

The versatility in the composition of the organic linkers and metal nodes and the possibility of post-synthetic modification, together with the large surface area and porosity

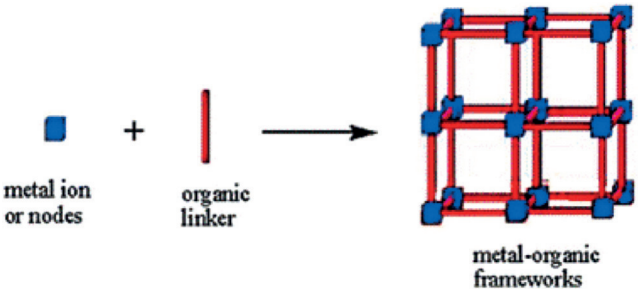

Figure 3. Building blocks and porous structure of a MOF.

Hermenegildo Garcia is full Professor at the Instituto de Tecnologi'a Qui'mica of the Technical University of Valencia and Honorary Adjunct Professor at the Center of Excellence in Advanced Materials Research of King Abdulaziz University. He was a postdoctoral researcher at the University of Reading with Andrew Gilbert and had several sabbatical leaves in the group of J. C. Scaiano in Ottawa. His research centers on heterogeneous catalysis with porous catalysts and nanoparticles. He is Doctor Honoris Causa from the University of Bucharest and the recipient of the 2011 Janssen-Cilag award and the 2008 Alpha Gold award.

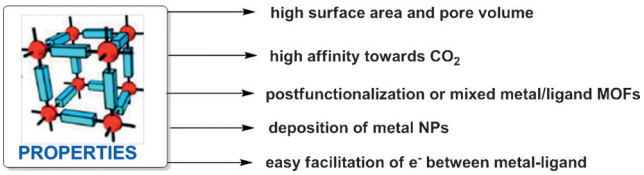

Figure 4. Some of the common properties of MOFs responsible for their photocatalytic activities.

allowing incorporation of guests means that in many respects MOFs (Figure 4) could be similar to zeolites and probably also semiconducting metal oxides.[35] However, in contrast to zeolites that are transparent to most visible and UV radiations, MOFs can play an active role, absorbing photons by the organic linkers and converting the initial ligand-localized exciton into a charge-separate state by single electron transfer from the ligand to the metal nodes (Figure 5). In MOFs, the most common ligands are aromatic

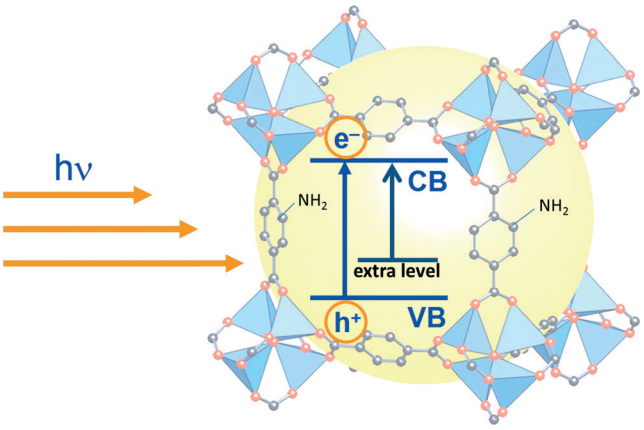

Figure 5. An illustration of the effect of -NH_2 substitution which adds an additional energy level to the band gap of MOFs that effectively decreases the band gap with respect to the unsubstituted MOF giving the MOF visible light photoresponse.

polycarboxylates which because of their excess of electron density can, upon photon absorption, transfer an electron to the positive metal ions bound to them. Other linkers can exhibit similar photochemical behavior and, therefore, the framework nature with linkers coordinated to metal ions, allows photoinduced electron transfer from the linker as electron donors to the metal nodes as electron acceptor to be quite a general process.[36–38] Moreover, aromatic compounds have intense absorption bands above 250 nm and depending on the substituents can easily move to 300 nm or even into the visible region ($\lambda > 400$ nm) and, therefore, MOFs can be designed in principle to exhibit visible-light photoresponses. Light absorption and photochemical excitation cannot occur in zeolites and (alumino)silicates in the absence of impurities, since they are transparent in the whole range of UV and visible radiation. The use of MOFs as photocatalysts is an emerging field[39] owing to the versatility of these materials and there are recent Reviews describing the activity of MOFs for the degradation of dyes,[40] water splitting,[41] and H_2 production or photocatalytic CO_2 reduction.[42]

By means of the appropriate substitution of common aromatic linkers or by selecting dyes as linkers, it is possible to design MOFs with a visible-light photoresponse at long wavelengths. This methodology to control the light-absorption properties is typical of organic molecules and, these concepts can be implemented easily in MOFs, but is not suitable for conventional inorganic semiconductors. A clear example of the influence of substitution is the general effect of the -NH_2 group as a substituent of 1,4-benzenedicarboxylic acid (bdc) and other aromatic polycarboxylates, where it introduces a new band in the visible with λ_{max} around 400 nm in the aminated MOF. The aminated MOF is isostructural with the parent unsubstituted MOF and can be synthesized by the same procedure (Figure 5). Other examples are the use of porphyrins or metal polypyridyl complex dyes as linkers forming a MOF with visible-light photoresponse characteristic of these chromophores. Moreover, it is not necessary to use a single linker in the synthesis of a MOF and mixed-linker MOFs having the unsubstituted and the -NH_2 substituted linker as building units can equally be prepared, exhibiting interesting photophysical properties.

Semiconductors are characterized by undergoing photoinduced charge separation and charge mobility, usually of one of the charge carriers. In n-type semiconductors, such as TiO_2, light absorption promotes electrons from the valence band (VB) to the conduction band (CB) and a fraction of them migrate away from the site at which the photophysical event took place, eventually reaching the external surface of the particles. As commented above, MOFs also undergo photoinduced charge separation and in some special cases the charge carriers have some mobility that is reflected in the long lifetime of these charge-separated states that can reach the microsecond timescale. Accordingly, most MOFs should not be considered as semiconductors because of their inefficient charge mobility, although a systematic study on the charge mobility in these materials would be much welcome.[13]

Concerning strategies to enhance charge mobility, it should be commented that some of the MOFs have chains of transition-metal atoms connected by oxygen bridges that resemble a 1D wire of inorganic semiconductors inside the crystal. One example of this type of structure is MIL-53 (Figure 6). It is possible that charge migration could take place preferentially in these 1D wires within the crystal has been determined for conventional semiconductors with 1D morphology, such as rods or tubes, that exhibit longer free-migration paths in along the long axis of the particles. Thus, it has been established by transient spectroscopy that the mobility of electrons along the long axis in TiO_2 nanotubes is much faster than perpendicular to it, along the short axis.[43]

However, even for those MOFs that do not contain a continuous chain of metal oxide motifs, charge mobility could take place if there is an adequate orbital overlap that can create a conduction band, in which charge carriers can migrate. In addition, those MOFs that contain nanometric clusters of metals offer the possibility to mimic some of the properties found in quantum dots. One of these cases is MIL-

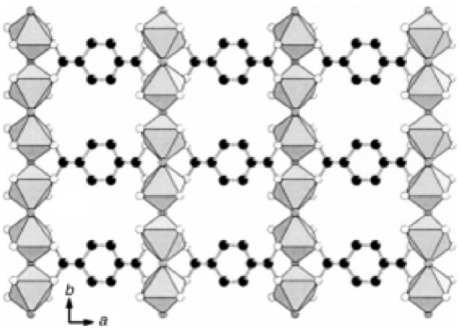

Figure 6. View of parallel, corner-sharing octahedral $MO_4(OH)_2$ chains running from top to bottom connected through the bdc ligands in MIL-53 (reproduced with permission from Ref. [44]).

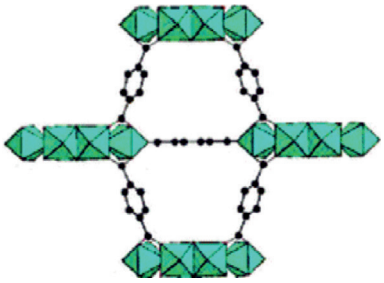

Figure 7. Simulation of part of the structure of MIL-125(Ti) in which the octamers of TiO_6 octahedra (in blue) sharing edges and forming perforated rings connected by bdc linkers can be seen (reproduced with permission from Ref. [45]).

125 containing rings of eight Ti edge-sharing octahedra (Figure 7).[45]

3. Photostability

One of the major limitations of MOFs is their lack of thermal stability at high temperatures, typically above 250 °C, which is a consequence of the type of coordinative metal–ligand forces responsible for the structure. Not only that, certain MOFs can be instable and their structure collapses in certain solvents or on contact with some reagents. Owing to the presence of metal ions and the nature of the forces, H_2O and polar solvents can cause structural damage in certain MOFs by metal-ion solvation. Reagents that can coordinate strongly with metal ions, such as strong nucleophilic species including hydroxide, amines, and alkoxides are likely to destroy MOF structures by competing favorably with the coordinative metal–linker bonds present in MOFs.

Besides this general remark concerning physical and chemical stability, for the specific case of their use as photocatalysts, the photochemical stability of the material is also the major issue. Organic molecules can commonly undergo fast degradation upon illumination or exposure to ambient conditions which cause some degree of photooxidation. Oxygen is a general quencher of electronic excited states, particularly, triplets, forming singlet oxygen that is a reactive species that can attack multiple bonds, polycyclic aromatic compounds, and benzylic and allylic positions. In addition, oxygen can undergo electron transfer with the excited states of organic molecules to form superoxide that is also a reactive species that results in the formation of hydroperoxides.[46,47] At least these two pathways can accelerate the oxidative degradation or the transformation of the organic linker. In addition, organic molecules also react photochemically with many other molecules, such as alcohols, amines, and alkenes.

The result of this reactivity is that the photochemical stability of MOFs should not be taken for granted, just based on their stability under dark conditions and has to be checked carefully when proposing MOFs as photocatalysts. Extended irradiation for long periods under conditions similar to that of their use as photocatalysts should be carried out and the stability of the MOF confirmed by X-ray diffraction, surface-area measurements, and spectroscopy. In one of the examples in which MOFs can degrade upon irradiation, CAU-8 with formula Al(OH)(bpdc) (bpdc: 4,4′-benzophenonedicarboxylate) loses its crystalline structure upon irradiation in CH_3OH by reaction of the bpdc linker, as determined by IR spectroscopy.[48] A good practice in this area would be to expose the MOF to intense irradiation in the presence of oxygen for months, checking periodically that the structure remains unaltered.

4. Design of MOFs as Photocatalysts

One of the major advantages of MOFs with respect to other materials is that their synthesis allows the incorporation of a large variety of linkers, transition metals, and structural arrangements. This variety means that it should be possible to select building blocks and target structures for a better performance of MOFs as photocatalysts. To have an efficient photocatalytic material, several requirements have to be met simultaneously. First, the material has to absorb light to undergo electronic excitation with the available light source. For many of the photocatalytic applications including degradation of environmental pollutants and photocatalytic fuel production, natural sunlight must be used as the excitation source. The percentage of the solar energy reaching the Earth′s surface corresponding to the UV region is about 4% and about 46% corresponds to the visible region. This distribution of energy determines that for photocatalytic systems that have to operate with natural sunlight it is highly recommendable to have a photoresponse to visible light in order to achieve high photocatalytic efficiencies with this natural light. For this reason, there are a large number of studies that specifically determine the photocatalytic activity of the material under artificial visible light considering that the photoresponse of the material to visible light will be more indicative of the behavior of the photocatalyst upon irradiation with solar light. For the use of MOFs as photocatalysts it is highly desirable to have linkers that absorb in the visible region. Since most of the benzene derivatives, including bdc absorb in the UV, the presence of substituents with strong bathochromic influence in the absorption is necessary. Particularly NH_2-groups, but also the use of polycyclic

aromatic compounds as linkers, shifts the response of MOFs towards the visible region (Figure 5). In addition, inorganic metal ions or metal oxide nodes can also act as visible-light harvesting centers. This concept has been demonstrated by subjecting a series of iron(III)-based MOFs which consist of Fe_3-μ_3-oxo clusters as visible-light photocatalysts for the degradation of Rhodamine 6G.[30] Furthermore, it is observed that crystallinity is not mandatory to achieve an efficient photocatalyst, since the poorly crystalline material Basolite F300, with only a local order around the Fe_3-μ_3-oxo clusters also shows photocatalytic activity.[30] Similarly, unprecedented 3d–4f MOFs, assembled with iodide-templates, were shown to be photocatalytically active under UV irradiation for the generation of H_2.[49]

In addition to light absorption, charge separation is the second elementary step in any photocatalytic event. In the case of MOFs, charge separation seems to be favorable because of the close contact and rigid positioning of linkers and metal modes (Figure 8). However, after charge separation, charge recombination between the same partners involved in photon absorption is a general deactivation pathway that is competing with photocatalytic activity.

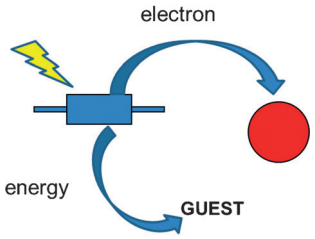

Figure 8. Schematic illustration of how photon absorption by the organic linker in a MOF (bipodal blue rectangle) can lead to energy transfer to occluded guests in close proximity to the linker or to electron transfer from the linker to the metal nodes (red circles).

At the moment there is a lack of information about the importance of charge recombination in MOFs. These data could be obtained by ultrafast transient absorption spectroscopy monitoring the primary species of charge separation and following their temporal evolution. The ratio between the initial numbers of charge separation species formed in the picoseconds time scale with those surviving up to the microsecond time scale should give a quantitative value of the percentage of charge recombination versus migration rates. Another important parameter is the density of charge carriers that can be determined, for instance, by photoelectrochemical measurements. These measurements should give an idea how fast charge carriers can move in the MOF crystal without undergoing recombination and also could serve to rationalize different photocatalytic behavior as a function of the composition and structure of the material. At the moment there is a lack of this fundamental information that together with the energy values of the electron and holes would serve to set up the fundamental basis of the photocatalytic behavior of MOFs. In addition, experimental characterization of the relevant photochemical parameters should be accompanied by theoretical calculations and modeling, thus, providing the basis for the understanding of the photocatalytic activity.

In the past three decades, numerous visible-light photocatalysts have been developed which include doped TiO_2,[50,51] hybrid photocatalysts composed of TiO_2 and other semiconductors,[52–55] photocatalysts based on the heterojunction of two semiconductors with different conduction and valence band energies[56,57] and dye-sensitized photocatalysts.[58,59] The main two issues encountered in all these studies aimed at producing efficient visible-light photocatalysts are 1) to reduce their absorption energy below 3 eV so that photocatalysis can be carried out under visible light and 2) to separate photogenerated electrons and holes minimizing their immediate recombination, thus, making it possible for these photogenerated carriers to trigger reduction and/or oxidation reactions.

To date, most of the reports in this area have tested as photocatalysts MOFs that have been previously described in the literature for other purposes. In some cases these already reported MOFs have been adapted for their use as photocatalysts. The two most common modifications have been the use of NH_2-containing linkers to increase visible-light photoresponse of the material as already commented and the deposition of Pt nanoparticles (NPs).

Even though the modification of MOFs to adapt their properties to their use as photocatalysts has been successful and surely many more examples will appear in the future, this approach does not fully exploit the flexibility that MOFs allow for design. It would be very important to show that new MOFs can be synthesized purposely for their specific use as photocatalysts, including steps of post-synthetic modification of MOFs mainly to introduce suitable co-catalysts. In the MOF design, the above commented requirements in terms of light-harvesting efficiency, particularly for solar-light irradiation, efficient charge separation, and high charge mobility should be taken in to account. The function of light harvesting could be performed by organic dyes, and metal centers that as discrete molecules in solution or as metal oxide clusters can absorb visible light. The charge separation step should take into consideration the redox potential of metal clusters and their orientation with respect to the LUMO orbitals of the linker. Probably, clusters of metals having several metal ions could be more appropriate for this purpose since they could store more than one electron as happens in the natural Mn_4 oxygen evolution center.[60] It is clear that charge accumulation is thermodynamically unfavorable and requires a thermodynamic cost that should be overcome by the potential of the photogenerated electrons and holes. The oxidation state of the metal ions should also influence in the efficiency. Charge mobility inside MOF crystals could require the existence in the structure of chains of metal-ion clusters that acting as wires can allow fast migration of charge carriers. For instance, the previously commented case of MIL-53 containing an array of infinite MO_6 (M: Al, Cr, Fe, Sc) octahedra chains connected by organic linkers at the equatorial position of each octahedra in the chain. These new concepts can lead to ideal types of MOFs for photocatalysis with suitable linkers, transition metals, and frameworks adapted for the specific use of photocatalysis. After the synthesis, post-

synthetic modification can include incorporation of metal NPs or even the combination of metal NPs for management of electrons, and of suitable metal oxides, such as RuO_2 or CeO_2, to favor hole transfer. Crystal size and surface modification should also be taken into consideration for enhancing photocatalytic activity. Surely, this concept will lead in the future to the synthesis of MOFs photocatalysts, synthesized by design. This approach of application-driven synthesis is unique for these type of materials since as commented in the Introduction most of the conventional photocatalysts are very difficult to adapt and variation of the synthesis conditions are less reliable or flexible as in the case of MOFs.

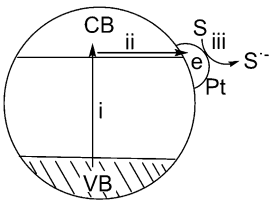

Figure 9. Pt NPs on the surface of a semiconductor can act as an electron acceptor of CB electrons, increasing the efficiency and lifetime of charge separation, and as co-catalyst transferring electrons to the substrate S. i) photoexcitation of the semiconductor with the promotion of one electron from the valence band to conduction band; ii) electron migration to the semiconductor particle surface and then to the Pt NP; iii) electron transfer from Pt NP to S.

5. Metal Nanoparticles in Photocatalytic MOFs

Noble-metal NPs can have a dual role in photocatalysis, acting as visible-light harvesters and as catalysts for the transfers of charge carriers from the semiconductor to the substrate.

Certain noble metals, when in nanometric size particles, may exhibit a characteristic absorption band in the visible region that arises from the collective oscillation of electrons confined in a cage of nanometric dimensions. This visible absorption band is termed a "localized surface plasmon band" and is observed for Au, Ag, and Cu.[61–64] The maximum absorption wavelength, the shape of the peak, and intensity of the surface plasmon band can be tuned by varying their size, morphology, and the environment experienced by the NPs.[65–67] Excitation of this surface plasmon band with visible light can produce the photoejection of "hot" electrons from the metal NP to the environment. A fraction of these photoejected electrons can be trapped by the photocatalyst electron-acceptor sites and can result in a long-lived charge separation where the positive hole is located at the metal NPs and the electron on the photocatalyst. Another effect of metal NPs excited with visible light is to produce strong electric fields in the neighborhood of the NP that can result in a more efficient charge separation in the photocatalyst. Both effects, photoejection of thermalized electrons and strong electric fields, can contribute to the visible-light photoresponse of a photocatalyst that otherwise would be inactive upon irradiation at the visible wavelengths corresponding to the light absorption of the metal NPs.

A second role played by noble-metal NPs in photocatalysis is to act as electron traps and active reaction sites.[68] When electrons cross the surface from the photocatalyst to the metal NPs, the lifetime of the charge-separated state increases, as a result of the difficulty of charge recombination. It is considered that also in the case of MOFs the presence of metal NPs can enhance the charge-separation efficiency by allowing migration of electrons from the MOF where they have been initially photogenerated to the metal NP acting as electron reservoir. Crossing surfaces ("Schotky barrier") from MOF to Pt NPs is a way to increase the distance moved by charge carriers and to increase the lifetime of the electrons by many orders of magnitude. Metal NPs can also act as co-catalysts transferring electrons efficiently to substrates. Figure 9 summarizes the presumed roles of Pt NPs as additives to photocatalysts. There is by now a sufficiently large number of reports showing that by making use of these two strategies, the photocatalytic efficiency of these modified MOFs is increased with respect to the parent MOF, frequently by several orders of magnitude.

Since noble-metal NPs act as electron reservoirs, they are typical co-catalysts for reductive reactions, such as the generation of H_2 from water. Photocatalytic reductions are the key half-reaction for the generation of solar fuels and noble-metal NPs are the general co-catalysts to enhance the efficiency of these processes.

The interest in adding metal NPs into the pores of MOFs is common in catalysis[69] and photocatalysis. Recently, several methodologies have been developed to incorporate metal NPs within MOFs.[70] Behind these strategies, the important issue is to have a clear understanding of the process of formation of NPs embedded in MOFs and which parameters are crucial to obtain samples that exhibit the optimal photocatalytic efficiency. Typically, the key issues are to achieve a uniform and small NP dimension, at the appropriate metal loading that does not compromise the surface area, pore dimensions, and volumes of the pristine MOF. Experimental parameters, such as metal precursors and amounts, reduction procedure, temperature, and time of the treatment have to be carefully controlled.

Among the most used deposition procedures, one that has shown a fine control of the metal NP size and distribution is the solid grinding of a volatile metal precursor that is subsequently thermally or chemically reduced into metal NPs.[71] Also methods in the liquid phase by adsorption of metal salts, followed by chemical reduction under conditions compatible with MOF stability have been also frequently used.[70] From the data in the literature, it appears that following appropriate procedures it is possible to incorporate, inside the MOF pores, particles with size limited by the pore dimensions of the crystal structure. Since small particle size is one of the crucial parameters for reaching high catalytic activity, encapsulation of metal NPs within MOFs is considered a powerful general strategy in heterogeneous catalysis to develop highly active catalysts.

Perhaps the most specific deposition procedure for the use of MOFs as photocatalysts is the so-called photodeposition method.[72] In this method the MOF is irradiated at the appropriate wavelength range in the presence of a precursor

of the noble metal dissolved in a convenient solvent containing a sacrificial electron donor. It is assumed that upon irradiation and generation of the charge-separated state, electrons should reduce the noble-metal precursor present in the solution leading to the formation of metal NPs onto the MOF pores. Sacrificial electron donors are typically methanol, ethanol, or tertiary amines. Amines are better electron donors than alcohols, but when using them the pH value of the solution has to be controlled to avoid damaging the MOF structure. Micromolar solutions of noble metals are commonly employed in these photodeposition processes to avoid depositing an excessive amount of metal. The main advantage of photodeposition with respect to other alternative deposition procedures is that metal NPs are located at the sites where electrons are located in the photocatalyst and, therefore, they should be more efficient for their role as electron acceptors and co-catalysts. In contrast, other alternatives should lead to the formation of metal NPs all over the MOF and the interfacial contact between MOF and metal NPs would presumably be lower.

Although the beneficial effects of the presence of noble-metal NPs for the photocatalytic activity of MOFs is well established, there are serious concerns on the practical applicability of photocatalysts having precious metals. Therefore, there is a need to find suitable materials that can act as sustainable and affordable alternatives to noble metals as co-catalysts. Certainly, new research in this area is necessary to meet the performance requirements.

6. Best Practices for MOFs as Photocatalysts

This Section presents some important general considerations to be taken into account when evaluating the activity of photocatalysts including MOFs. One major issue is how to compare photocatalytic-activity data from different laboratories for different materials. Part of the problem derives from the insufficient characterization data of the material being tested and the reproducibility of the synthesis. Data such as the crystallinity of the sample, elemental composition and the possible presence of impurities, surface area, and particle size should be routinely given.

The efficiency of photochemical reactions for soluble compounds can be determined in an absolute way by providing quantum yields that are the ratio between the number of photoproduct molecules formed and the number of absorbed photons. However, measurements of absolute quantum yields for solids are not possible because of light scattering and reflection. Nevertheless a useful parameter is the incident light to photoproduct conversion that is equivalent to the way in which solar cells efficiencies are given.[73,74] These apparent quantum yields can vary with those parameters that influence light scattering, such as particle size and photoreactor design, but at least provide a quantitative value of the efficiency of the photocatalytic process.

Another piece of information that is important to evaluate the performance of a photocatalyst is the photoresponse of product formation as a function of the irradiation wavelength. In principle, the photoresponse should coincide with the absorption spectrum of the chromophores responsible for the photocatalytic activity and, therefore, the photoresponse provides useful information on the operation mechanism. As commented earlier, a constant target in solar photocatalysis is to develop materials with a photoresponse in the visible region ($\lambda > 380$ nm) and even in the near-infrared ($1500 > \lambda > 800$ nm), where solar light irradiance mostly occurs. In the absence of photoresponse data, the use of suitable cut-off filters can serve to determine the visible or near-infrared photoresponse of a photocatalyst.

Besides the material, the efficiency of a photocatalytic process is strongly influenced by the irradiation source and photoreactor design. For the purpose of solar fuel production, solar simulators with appropriate filters or even direct sunlight irradiation should be performed. Curiously, activity data for direct sunlight irradiation are less recommendable in terms of reproducibility because of changes in solar irradiance depending on the season, weather conditions, daytime, and height and latitude of the irradiation. Many MOFs exhibit photocatalytic activity upon excitation in the UV region and this requires the use of lamps, such as low- or medium-pressure Hg arc lamps emitting at 254 nm in a more or less continuous way.

Photoreactors have to be designed in combination with the light source for an efficient use of the emitted photons. Photoreactors for gas evolution have to be sealed and should allow periodic sampling of the gas and liquid phase. Oxygen has to be avoided in the system, since this molecule is an efficient quencher of electrons and will impede photoreduction of any other substrate in its presence. The best practice is to perform irradiations for the production of H_2, CH_4, and other gases under a continuous flow of inert gas and analyze the out stream directly with in-line chromatography. In this way, errors derived from manipulation and quantification of gases are minimized.

In addition, photostability of the solid acting as the photocatalyst should be provided, by performing prolonged irradiation tests evaluating the temporal evolution of the photoproducts. During these stability tests, any leaching of metal or organic linker from the solid to the solution should be determined by chemical analysis of the liquid phase after filtration of the solid photocatalyst and also the spent photocatalyst must be submitted for suitable analysis. Elemental data should be compared to those of the fresh MOF. Also crystallinity, surface area, and particle morphology should be checked for the used material by X-ray diffraction, gas adsorption, and electron microscopy, respectively and compared to the data for fresh samples. Recyclability tests in which the photocatalyst is recovered after a run and reused in a subsequent reaction should also be performed, monitoring the temporal evolution of the photoproducts. Photocatalyst deactivation can be determined by lower initial reaction rates and lower photoproduct formation at a certain irradiation time under the same conditions. The cause of deactivation should be determined by comparing data of fresh and used photocatalyst. In the particular case of MOFs, decrease in the crystallinity and porosity are the two most common specific reasons for deactivation.

Photocatalysis for solar fuel production is a reduction process. To determine the maximum efficiency of solar fuel production it is a common practice to perform the reaction in the presence of a sacrificial electron donor agent, such as methanol or a tertiary amine. Since in the photoinduced charge separation, electrons and holes are simultaneously generated in the same amount, the electroneutrality principle requires that the consumption of these charges should take place in the same stoichiometry and rate. Sacrificial electron donors ensure that the rate of hole consumption is not the rate-determining process and these conditions are the optimal to establish the highest efficiency in photoreduction. From the practical point of view of solar fuel production, these conditions are generally unrealistic, since the electron donor in natural photosynthesis is water.[75] Compared to tertiary amines, water is a poor electron donor and the photooxidation half-reaction becomes the rate determining process for most of the photocatalysts, lowering the efficiency of solar fuel production by several orders of magnitude. In the case of MOFs as photocatalysts, the use of sacrificial electron donors may not be a good choice, because of the lack of stability of most MOFs in the presence of amines or in water at basic pH values. In addition, the photocatalytic activity should be increased by incorporation of noble metals in optimal amounts as co-catalysts to increase the photoreduction reaction rate.

The final goal of the area is to develop a photocatalyst and a process that can produce solar fuels competitively at the current prices of energy. Therefore, evaluation of the photocatalytic activity of a promising material should also include data on the overall water splitting and photochemical CO_2 reduction by water. In both processes water is the source of electrons.

In addition to these general considerations, there are specific issues for each photocatalytic reaction, such as for instance, in the case of the overall water splitting how to separate evolved oxygen from H_2. Some of these points will be discussed below, when presenting the results reported using MOFs as photocatalysts.

7. Summary of the use of MOFs as Photocatalysts for H_2 Generation and CO_2 Reduction

The following Sections will describe examples reported in the literature showing the photocatalytic activity of MOFs for H_2 generation and CO_2 reduction. The Review is organized by presenting the use of MOFs in photocatalytic H_2 generation (Table 1), CO_2 reduction (Table 2), and photooxygenation (Table 3) and nitro reduction. Throughout the Review the components and organization of the heterostructures based on MOFs will be presented in a schematic way. Whenever possible, the issue of catalyst stability after a photochemical reaction has been discussed and a suitable comment is also given for future directions. Application of MOFs in the photodegradation of dyes or environmental pollutants is out of scope of the present Review. The reader is referred to a recent Review for a deeper coverage of the fundamentals and models of the energy transfer in MOFs as photocatalysts,[39] which subset of MOFs can be considered as semiconductors,[13] as well as the use of specific MOFs as photocatalysts.[76–79]

8. MOFs as Photocatalysts for H_2 Generation

Pt NPs are very general co-catalysts for H_2 generation in metal oxide semiconductors and their presence increases the photocatalytic activity. The same general effect is now well-documented also for MOF photocatalysts. To observe their beneficial influence, Pt NPs have been loaded into stable, porous, and phosphorescent MOFs built from $[Ir(ppy)_2(bpy)]^+$-derived dicarboxylate ligands (ppy = 2-phenylpyridine; bpy = 2,2′-bipyridine) and $Zr_6(\mu_3\text{-}O)_4(\mu_3\text{-}OH)_4$ $(carboxylate)_{12}$ as secondary building units. Deposition of Pt NPs was performed via MOF-mediated photoreduction of K_2PtCl_4.[80] The resulting Pt@MOF-1 or Pt@MOF-2 assemblies were investigated as effective photocatalysts for H_2 evolution by photoexcitation of the MOF frameworks under visible light ($\lambda > 420$ nm). $Zr_6(\mu_3\text{-}O)_4(\mu_3\text{-}OH)_4(bpdc)_{5.94}(L_1)_{0.06}$ (MOF-1) was prepared by post-synthetic modification of the L_1 (Scheme 3) ligand into the preformed UiO-67 framework having bpdc as the bridging ligand at approximately 2 wt% loading.[80] MOF-2 was synthesized by treating L_2 (Scheme 3)

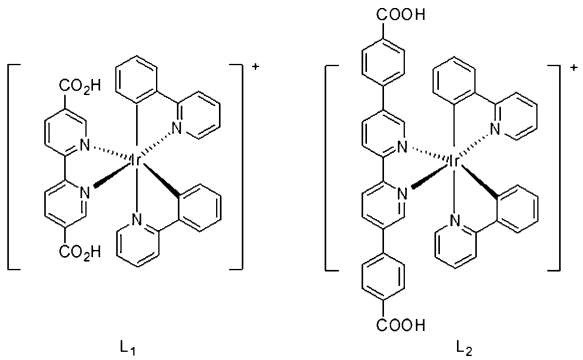

Scheme 3. Chemical structures of L_1 and L_2 used to construct MOF-1 and MOF-2.

with $ZrCl_4$ in DMF, obtaining a solid with the formula $Zr_6(\mu_3\text{-}O)_4(\mu_3\text{-}OH)_4(L_2)_6 \cdot 64$ DMF. HRTEM analysis revealed that after photodeposition the cavities of MOF-1 and MOF-2 contained Pt NPs with diameters of 2–3 and 5–6 nm, respectively. The fact that the Pt NPs sizes are larger than those of the MOF cavities indicates partial MOF framework distortion/degradation during Pt NP formation, although it could also be possible that the Pt NPs extend through more than one cavity. The Pt/Ir ratio in the MOF sample was determined to be 18.6 and 17.8 for Pt@MOF-1 and Pt@MOF-2, respectively by ICP-MS. The highest turnover number (TON) achieved for H_2 evolution based on Ir content (Ir-TON) is 730 and 1620 for Pt@MOF-1 and Pt@MOF-2, respectively after 6 h. The Ir TONs of the recovered Pt@MOF-1 were 633, 624, and 749 for the 2nd, 3rd, and 4th run, respectively. The Ir TONs observed for H_2 evolution rate using Pt@MOF-2 for 1st, 2nd, 3rd, and 4th runs were 1620,

Table 1: Summary of photocatalytic reactions on H_2 evolution, CO_2 reduction, and photocatalytic organic synthesis using various MOFs-based catalysts.[a]

Photocatalyst	Light source (sacrificial agent)	Photoactivity	Stability evidence	Ref.
Photocatalytic H_2 evolution				
Pt@MOF-1 or Pt@MOF-2	450 W Xe-lamp (TEA), Visible	3400 or 7000 TON	reuse, leaching	[80]
H_2TCPP[AlOH]$_2$(DMF_3-$(H_2O)_2$)	300 W Xe lamp (EDTA), Visible	200 μmol g^{-1} h^{-1}	SEM, XRD	[81]
{[$Ln_2Cu_5(OH)_2(pydc)_6(H_2O)_8$]·$I_8$} (Ln: Tb)	500 W Hg lamp (aq. CH_3OH), UV	2105 μmol h^{-1} g^{-1}	reuse, IR, XRD	[49]
MOF-253-Pt	300 W Xe lamp (TEOA), Visible	3000 μmol	reuse	[82]
Pt/NH_2-UiO-66	200 W Xe-doped Hg lamp(CH_3OH)	2.8 mL	–	[83]
NH_2-UiO-66(Zr/Ti)-120-16 days	300 W Xe lamp (CH_3CN and TEOA)	3.5 mmol mol^{-1}	–	[84]
RhB/UiO-66(Zr)-100*	300 W Xe lamp (TEOA)	33.9 μmol g^{-1} h^{-1}	XRD	[85]
Pt-UiO-66-30	300 W xenon lamp (20% CH_3OH)	37 μmol	reuse, ICP-AES	[86]
Pt/Ti-MOF-Ru(tpy)$_2$	500 W Xe lamp (TEOA)	5.1 μmol	reuse, XRD	[87]
Pt/[Cu(en)$_2$]$_4$[$PNb_{12}O_{40}(VO)_6$]· $(OH)_5$·8 H_2O	125 W Hg lamp (aq.CH_3OH)	44.35 μmol g^{-1} h^{-1}	XRD	[88]
Fe_2O_3@TiO_2/Pt	Xe lamp (TEA)	0.8 μmol	EDS, TEM, XRD, reuse	[89]
Pt@CdS/MIL-101(Cr)	300 W Xe lamp (lactic acid)	150 μmol h^{-1}	reuse, XRD	[90]
UiO-66/CdS/rGO	300 W Xe lamp (aq. 0.1 M Na_2S and Na_2SO_3)	105 μmol h^{-1}	XRD	[91]
Pt/NH_2-MIL-125(Ti)	Xe lamp (TEOA)	33 μmol	reuse, BET, XRD	[92]
Pt(1.5)/NH_2-MIL-125(Ti)	500 W Xe lamp (TEOA)	15.5 μmol	reuse	[93]
Pt/MIL-125(Ti)	Xe lamp (λ = 320-780 nm) (TEOA)	38.68 μmol	–	[94]
Co@NH_2-MIL-125(Ti)	500 W Xe/Hg lamp	37 μmol	reuse	[95]
Photocatalytic CO_2 reduction				
NH_2-MIL-125(Ti)	Xe lamp (CH_3CN/TEOA)	8.14 μmol $HCOO^-$	XRD, BET, TGA, IR, Raman	[96]
Au/NH_2-MIL-125(Ti) or Pt/NH_2-MIL-125(Ti)	300 W Xe lamp (TEOA)	9.06 μmol or 12.96 μmol $HCOO^-$	–	[97]
NH_2-UiO-66	500 W Xe lamp (TEOA)	13.2 μmol $HCOO^-$	XRD, IR, BET	[98]
NH_2-UiO-66(Zr/Ti)-120-16 days	300 W Xe lamp (CH_3CN and TEOA)	5.8 mmol mol^{-1}	XRD, BET	[84]
$Zr_{4.3}Ti_{1.7}O_4(OH)_4(C_8H_7O_4N)_{5.17}(C_8H_8O_4N_2)_{0.83}$	300 W Xe lamp (CH_3CN and TEOA)	33 μmol $HCOO^-$	reuse	[99]
MIL-101(Fe) or NH_2-MIL-101(Fe)	300 W Xe lamp (CH_3CN and TEOA)	59 or 178 μmol $HCOO^-$	reuse, XRD, IR, TGA, BET	[100]
Cu porphyrin (5,10,15,20-tetrakis(4-carboxyphenyl)	300 W Xe lamp (TEA)	262.6 ppm g^{-1} h^{-1} CH_3OH	–	[101]
MOF-253-Ru$(CO)_2Cl_2$	Xe lamp (CH_3CN and TEOA)	0.67 μmol $HCOO^-$	XRD	[102]
Cp*Rh@UiO-67	300 W Xe arc lamp (CH_3CN and TEOA)	47 TON	reuse	[103]
Cu_3(BTC)$_2$@TiO_2	300 W Xenon (H_2O)	2.64 μmol $g_{TiO2}{}^{-1}$ h^{-1} of CH_4	reuse	[104]
CdS/Co-ZIF-9	300 W Xe lamp (TEOA)	CO (50.4 μmol h^{-1}), H_2 (11.1 μmol h^{-1})		[105]
g-C_3N_4 + Co-ZIF-9	Xe lamp (H_2O, CH_3CN, TEOA)	20.8 μmol CO	reuse	[106]
ZIF-8/Zn_2GeO_4	500 W Xe arc lamp	2.44 μmol g^{-1} CH_3OH	XRD	[107]

[a] Abbreviations: MOF-1: $Zr_6(\mu_3\text{-}O)_4(\mu_3\text{-}OH)_4(bpdc)_{5.94}(L_1)_{0.06}$; MOF-2: $Zr_6(\mu_3\text{-}O)_4(\mu_3\text{-}OH)_4(L_2)_6$·64DMF; TEA: triethylamine; PMOF: porphyrin MOF; EDTA: ethylenediminetetraacetic acid; TEOA: triethanolamine; bpdc: biphenyldicarboxylate; tcpp: *meso*-tetra(4-carboxylphenyl)porphyrin; Ln = Sm, Eu, Gd and Tb; pydc: pyridine-2,5-dicarboxylic acid; tpy: terpyridine; en: ethylenediamine; rGO: reduced graphene oxide; BTC: 1,3,5-benzenetricarboxylate.

1500, 990, and 1380, respectively, after 6 h. Pt@MOF-1 and Pt@MOF-2 samples reached an accumulated Ir TON of 3400 and 7000, respectively. These TON values measured for Ir-MOFs are 1.5- and 4.7-times the values afforded by the homogeneous controls [Ir(ppy)$_2$(bpy)]Cl/K_2PtCl_4 under comparable conditions (2200 and 1500, respectively). It was believed that the enhanced photocatalytic H_2 evolution activities of Pt@MOFs are due to a more efficient electron transfer from the photochemically unstable [Ir^{III}(ppy)$_2$-(bpy$^{\cdot-}$)] intermediate immobilized near Pt NPs which not only increased H_2 reduction rates, but also slowed down the decomposition of the Ir complexes. Photodecomposition is one of the major limitations of the Ir complex as a molecular photocatalytic system. The photodecomposition rate is directly correlated to the lifetimes of this species and should be disfavored when there is an efficient quenching pathway. Furthermore, this high instability of Ir(ppy)$_2$(bpy) is responsible for the Ir leaching into the solution that can reach 25.6% after 48 h of photocatalytic H_2 generation for Pt@MOF-2.

Porphyrins are the major constituent of natural photosynthetic centers in green plants. Not surprisingly, porphyrins can also act as light harvesters and photoredox centers for the generation of H_2. In this context, the reaction of $AlCl_3$·6 H_2O with tcpp (tcpp: *meso*-tetra(4-carboxylphenyl) porphyrin, Scheme 4) leads to the formation of the water-stable microcrystalline, porous, red compound H_2TCPP[AlOH]$_2$-

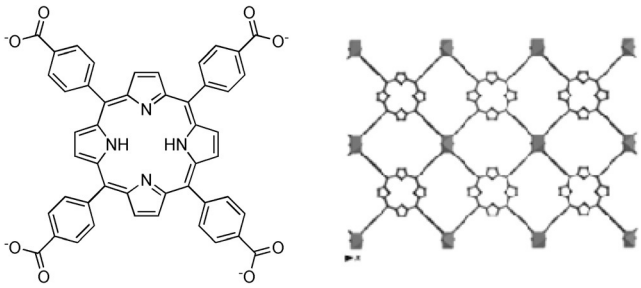

Scheme 4. Chemical structure of TCPP linker (left) and illustration of the structure of Al-PMOF (right; reproduced with permission from Ref. [81]).

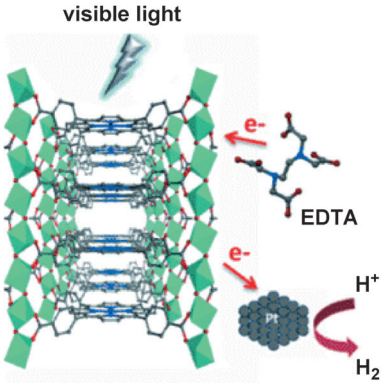

Scheme 5. Illustration of the mechanism of the photocatalytic H_2 generation upon visible-light irradiation of Al-PMOF using EDTA as sacrificial electron donor (reproduced with permission from Ref. [81]).

(DMF_3-$(H_2O)_2$) (Al-PMOF), whose photocatalytic activity for H_2 generation has been investigated under visible-light irradiation from H_2O using EDTA as the sacrificial electron donor.[81] The solid-state UV/Vis absorption spectrum of Al-PMOF showed the strong Soret band at 415 nm and four Q bands at lower energies, characteristic for free-base porphyrin.[108] On the other hand, the fluorescence spectrum displayed a band at 660 nm. Reaction of Al-PMOF with anhydrous $Zn(OAc)_2$ afforded a highly crystalline purple material with formula $Zn_{0.986}$TCPP-$[AlOH]_2$ consistent with over 90% occupancy of the porphyrin centers by Zn^{2+} as evidenced by energy-dispersive X-ray spectroscopy recorded by SEM. The BET surface area was measured to be of 1200 $m^2 g^{-1}$. UV/Vis spectrum of $Zn_{0.986}$TCPP-$[AlOH]_2$ confirmed the insertion of Zn^{2+} ions by observing a slight red shift in the Soret band to 425 nm from 415 nm for Al-PMOF and the predominant presence of only two Q bands (instead four for Al-PMOF) due to the higher symmetry of the metalated porphyrin with respect to the free-base porphyrin. Similarly, the fluorescence spectrum of $Zn_{0.986}$TCPP-$[AlOH]_2$ also reflects the effects of porphyrin metalation on the emission by displaying two maxima at 620 and 660 nm.

Two different approaches were employed to apply porphyrin MOFs (PMOFs) as photocatalysts, one is by taking advantage of the quenching of porphyrin-based excited states by methyl viologen (MV^{2+}) and the other approach is based on changing the amount of external colloidal Pt. First, the MOF/MV^{2+}/EDTA/Pt system was studied. In this case MV^{2+} acts as an electron acceptor and mediates the electron transfer from the excited state porphyrin to the colloidal Pt located outside the pores of the MOF. EDTA acts as the sacrificial electron donor restoring the Zn porphyrin radical cation moiety to the ground state. In this mechanism, MV^{2+} should be readily adsorbed by Al-PMOF or $Zn_{0.986}$TCPP-$[AlOH]_2$ in aqueous media and EDTA should be able to access the internal oxidized porphyrin species. Following visible-light absorption by zinc porphyrin and the generation of the associated electronic excited species, the MV^{2+} is reduced to the radical cation ($MV^{+\bullet}$) by electron transfer from the excited porphyrin, resulting in a positively charged porphyrin intermediate (Scheme 5). This positive Zn porphyrin reacts with EDTA that becomes oxidized to its corresponding radical cation and decomposes to degradation products. $MV^{+\bullet}$ should then migrate outside the MOF crystal, carrying one electron that should be transferred to the Pt colloid, evolving H_2 from H_2O. However, for both Al-PMOF and $Zn_{0.986}$TCPP-$[AlOH]_2$, this strategy gave only a small amount of H_2 upon illumination with visible light in aqueous EDTA/MV^{2+}/colloidal Pt solution for 15 h. This poor performance was explained by the inefficient diffusion of MV^{2+}/$MV^{+\bullet}$ redox pair through the pores, as the Pt NPs are too large to enter the pore system.

In contrast, a second set of experiments was performed with the PMOF/EDTA/Pt system in the absence of MV^{2+}. Using this in principle simple strategy, the excited porphyrin molecules in the MOF react directly with EDTA to form the reduced porphyrin which in turn transfers an electron to Pt. The Pt concentration was increased to ensure the optimum contact between the metal and the framework. Al-PMOF and $Zn_{0.986}$TCPP-$[AlOH]_2$ produced 200 and 100 $\mu mol\, g^{-1} h^{-1}$ H_2, respectively, after an induction period of about 3 h. Repeated reactions with the same catalysts showed good data reproducibility. Powder XRD and SEM measurements revealed that the framework remains unaffected after the photocatalytic reactions for both catalysts. Furthermore, heterogeneity was also confirmed, thus showing the higher stability of these MOFs under photocatalytic reaction conditions. Although in principle it may seem that saving MV^{2+} simplifies the system and achieves higher efficiency, this is at the expense of higher Pt concentrations. It seems, however, that the photocatalytic activity could have been further improved by incorporating Pt NPs inside the MOF pores.

A series of isomorphous MOFs with a molecular formula of $\{[Ln_2Cu_5(OH)_2(pydc)_6(H_2O)_8]\cdot I_8\}$ (Ln = Sm, Eu, Gd, and Tb) was synthesized.[49] The lattice defines triangular pores in which polyiodide chains acting presumably as templates in the synthesis of the MOF are located (Figure 10). Interestingly, these Ln MOFs exhibit high framework stability in acid or basic aqueous solutions.

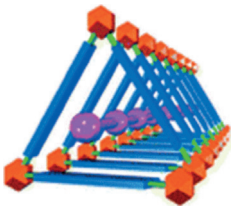

Figure 10. View of the triangular channels defined by the structure of $[Ln_2Cu_5(OH)_2(pydc)_6(H_2O)_8]\cdot I_8$ showing the incorporated polyiodide chain (reproduced with permission from Ref. [49]).

Optical band gaps of 3.12, 3.16, 3.15, and 2.82 eV were determined for the MOFs of Sm, Eu, Gd, and Tb, respectively. The photocatalytic H_2 evolution of Ln MOFs was evaluated in 10% aqueous CH_3OH solution under UV irradiation.[49] The H_2 evolution mean rates were 1958.0, 2262.8, 2050.4, and 2105.0 $\mu mol\,h^{-1}\,g^{-1}$, and the total H_2 amounts evolved during 5 h were 979.0, 1131.4, 1025.2, and 1052.5 μmol, for Sm, Eu, Gd, and Tb, respectively. The H_2 evolution activity of MOF with Gd was evaluated in six runs. The H_2 evolution rates in the first three cycles were 2050.4, 2107.7, and 1973.9 $\mu mol\,h^{-1}\,g^{-1}$ and the total H_2 evolved over 15 h was 3066 μmol. It was observed that the H_2 evolution rate in the third reuse was lower. However, IR and powder XRD spectra of the fresh and reused photocatalysts did not show any significant change indicating that no structure deterioration is taking place during the recyclability. It is unclear, however, if the polyiodide chains that are present in the structure and that can be released in CH_3OH play or not any role in the photocatalysis. This point should be clarified in view of the general use of triiodide as redox electrolyte in dye-sensitized solar cells.[15]

A new bifunctional MOF-253-Pt has been prepared by post-synthetic modification of uncoordinated bpy linkers in MOF-253 with Pt ions. The resulting photophysical Pt complex acts as a molecular photocatalyst for the reduction of H_2O into H_2 under visible-light irradiation.[82] The photocatalytic activity of MOF-253-Pt (0.53 mM based on Pt) was evaluated for H_2 evolution in the presence of 15 vol% TEOA as the sacrificial electron donor in H_2O at pH 8.5 under visible-light irradiation ($\lambda > 420$ nm). It was observed that the H_2 production increased proportionally with time upon light irradiation, and then gradually reached a plateau at about 30 h of 3000 μmol in a H_2O/CH_3CN mixture and to 1400 μmol in H_2O. It would be of interest to determine the reasons why H_2 generation stops and, particularly if the photocatalyst becomes finally deactivated. In contrast, control experiments showed that no H_2 evolution is observed under the same experimental conditions without MOF-253-Pt or in the absence of TEOA in the solution. The H_2 evolution rate decreased under both more acidic and more basic reaction conditions. It was observed that the H_2 evolution rate increases significantly along with the concentration of Pt in MOF-253-Pt. The photocatalytic activity also depends on the concentration of the TEOA as the sacrificial electron donor. At the constant catalyst concentration, the amount of H_2 evolved decreased to 80% when the concentration of TEOA decreased from 15 to 5%, reflecting the decrease in the quenching efficiency of the excited states when the concentration of TEOA becomes lower. In contrast, the amount of H_2 production achieved using MOF-253-Pt under identical experimental conditions was 4.7-times higher than that of the complex $Pt(bpydc)Cl_2$ that is the molecular analogue of the active center in MOF-253-Pt. The enhanced photocatalytic H_2 evolution activity of MOF-253-Pt with respect to the homogeneous complex could be attributed to a combination of beneficial effects present in the rigid MOF-253 structure including favorable interactions of spatially close Pt···Pt pairs, a more efficient electron transfer within the porous framework containing the metal complexes with respect to the molecular complex analogue, as well as a slowing down of the decomposition of the anchored $Pt(bpy)Cl_2$ complex within the MOF. The relative contribution of some of these possible effects could have been differentiated if the time–conversion plots would have been analysed and by determining if the differences between the performance of the MOF or the metal complex occur at initial reaction times or at longer times when deactivation of the fresh catalyst can take place. Furthermore, photocatalytic H_2 evolution using MOF-253-Pt was evaluated in the presence of mercury, observing that the presence of this Pt poison does not significantly affect the photocatalytic activity, thus, ruling out the formation of Pt NPs during the course of the reaction. The H_2 production rate in the 1st and 2nd reuse was around 170 and 85 μmol after 5 h using MOF-253-Pt in mixed solvent of $CH_3CN/TEOA/H_2O$ (17:2:1) at pH 8.5.

Considering the high thermal stability[109,110] and robust nature of UiO-66(Zr) in aqueous conditions,[111] this MOF is a good choice to begin to develop photocatalytic systems for H_2 production. In one of the first reports on the photocatalytic activity of MOFs, the Zr-containing MOFs, UiO-66 and NH_2-UiO-66 were tested as water-resistant MOFs in the photocatalytic activity for H_2 generation in CH_3OH or H_2O/CH_3OH (3:1) using a 200 W xenon-doped Hg lamp.[83] The materials UiO-66 and NH_2-UiO-66 are isoreticular as determined by the complete coincidence of the diffraction peaks from powder XRD. This indicates that the presence of the $-NH_2$ groups at the organic linker does not have any influence on the structure of the MOF and that the $-NH_2$ groups should be protruding into the empty space of the micropores. However, it seems that the presence of $-NH_2$ is key for the photocatalytic activity of UiO-66. Apparently the presence of $-NH_2$ introduces a new band in the visible region around 420 nm that is absent in the parent UiO-66. In a certain way, the influence of $-NH_2$ groups in MOFs in general is reminiscent to doping in classical metal oxide semiconductors which introduces a new state in the intraband-gap space leading to an effective shortening of the band-gap energy. Visible-light irradiation of UiO-66 suspensions in CH_3OH/H_2O did not result in H_2 evolution. Also, no H_2 was detected using UiO-66 as a photocatalyst in the absence of a sacrificial electron donor with Pyrex filtered UV light as excitation source. In contrast, photocatalytic generation of H_2 was observed using Pyrex filtered UV light as a radiation source in H_2O/CH_3OH mixtures. As expected, in view of its well-established role as a co-catalyst, the presence of Pt on UiO-66 and NH_2-UiO-66 significantly increased the initial reaction rate and the total amount of H_2 evolved during the course of reaction. The maximum amounts H_2 obtained for Pt/UiO-66 and Pt/NH_2-UiO-66 were 2.4 and 2.8 mL, respectively, after 3 h. In contrast, 4.5 mL of H_2 was obtained using the same weight of platinized TiO_2 (P 25) as a photocatalyst under identical experimental conditions. A control experiment further confirmed that one of the possible byproducts formed in the oxidation of CH_3OH, namely HCOOH, acts as a poison deactivating the catalyst. This could be one of the reasons why the catalysts become deactivated during operation. Furthermore, it was shown that CH_3OH is the most likely source of H_2 by dehydrogenative oxidation ("photo-

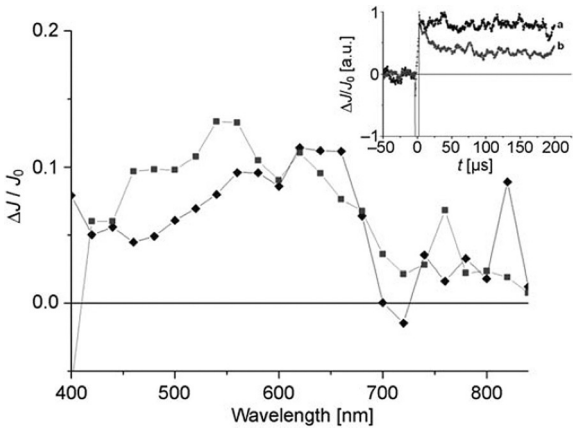

Figure 11. Time-resolved transient signal recorded 9.5 μs after 355 nm laser flash corresponding to the photogenerated charge separation state in UiO-66 (◆) and NH_2-UiO-66 (■). Inset: Temporal profiles of the transient spectrum of NH_2-UiO-66 monitored at a) 480 and b) 560 nm, showing different profiles indicating that they should correspond to different charge carriers (reproduced with permission from Ref. [83]).

reforming"), but however, the presence of H_2O enhances the photocatalytic activity. Also, spectroscopic evidence based on laser flash photolysis supported that Zr-MOFs can undergo long-lived charge separation (Figure 11). As commented in the Introduction, charge separation together with charge-carrier mobility are the genuine prerequisites of semiconductors.[112] However, it should be noted that comparisons of the photocatalytic activity of disparate materials (TiO_2 and MOFs) based exclusively on their weight can serve only as rough quantitative indicators of the activity that is always more accurately described in terms of TON when the nature of the active sites are known along with absolute quantum yield efficiencies.

While the most common UiO-66 material is based on Zr^{4+}, the most widely used semiconductor is TiO_2 so it would be of interest to check the photocatalytic activity of a Ti^{4+} analogue. The flexibility in MOF synthesis makes possible the preparation of Ti-containing UiO-66. Thus, the photocatalytic activity of NH_2-UiO-66(Zr/Ti)-120-16 derived from post-synthetic exchange of Zr by Ti in NH_2-UiO-66(Zr) was investigated in H_2 generation.[84] Inductively coupled plasma (ICP) analysis of NH_2-UiO-66(Zr/Ti)-120-16 (where 120-16 refers to 120 °C for 16 days for the exchange conditions) revealed that about 48.7 % of Zr in NH_2-UiO-66(Zr) was replaced by Ti after 16 days exchange. The photocatalytic activity of NH_2-UiO-66(Zr/Ti)-120-16 was tested in H_2 evolution with TEOA as an electron donor under visible-light irradiation. It was shown that 2.4 mmol mol^{-1} H_2 was detected over Pt/NH_2-UiO-66(Zr) after 9 h under visible-light irradiation. On the other hand, Pt/NH_2-UiO-66(Zr/Ti)-120-16 gave 3.5 mmol mol^{-1} of H_2 under similar conditions, which is 1.5 times that evolved over Pt/NH_2-UiO-66(Zr). These results open the door for the preparation of mixed-metal MOFs with two or more metal ions that can exhibit enhanced photocatalytic activity.

Besides direct excitation of the semiconductor, one general strategy to introduce visible-light photoresponse in photocatalysis is the use of dyes as photosensitizers. In this methodology, photons are absorbed by the dye that undergoes photoexcitation and injects one electron from its LUMO band to the CB of the semiconductor. This approach has been successfully applied to the development of dye-sensitized solar cells, but also in photocatalysis in general (Figure 2).[15] In this context, the visible-light photocatalytic H_2 production of Pt@UiO-66(Zr) sensitized by RhB dye using TEOA as electron donor has been reported (Figure 12).[85]

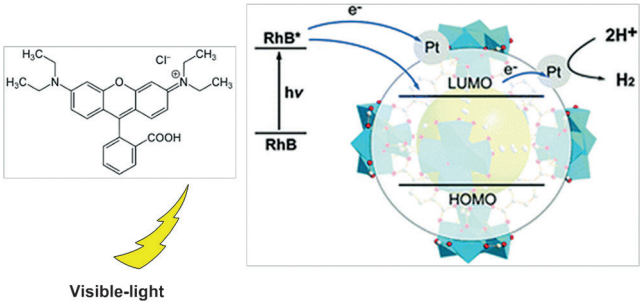

Figure 12. Pictorial illustration of RhB sensitization of a Pt@UiO-66-(Zr) (reproduced with permission from Ref. [85]).

The HRTEM images revealed the presence of Pt NPs with a particle size ranging between 3 to 5 nm dispersed over UiO-66(Zr). Although photocatalytic H_2 production has been reported using UiO-66(Zr)[83] under UV irradiation by a Xe-doped Hg lamp, no appreciable H_2 evolution was detected over pure UiO-66(Zr) under visible-light irradiation. Interestingly, 1 wt % Pt@UiO-66(Zr) showed a rate of 3.9 μmol g^{-1} h^{-1} H_2 production. RhB/UiO-66(Zr)-10 (1.63 mg g^{-1} of RhB adsorbed) in the absence of Pt NPs exhibited a comparable photocatalytic activity of 2.7 μmol g^{-1} h^{-1}. In addition, an increase in the loading of RhB on UiO-66(Zr) (7.43 mg g^{-1} for RhB/UiO-66(Zr)-100) does not lead a significant increase in the H_2 evolution rate. In contrast, when the same amount (7.43 mg g^{-1}) of dye was directly added into the solution just before light irradiation (RhB/UiO-66(Zr)-100*), the photocatalytic activity reached to 33.9 μmol g^{-1} h^{-1}. These results clearly show that RhB in solution can effectively sensitize UiO-66(Zr) and more interestingly, the amount of dye has a large influence on the photocatalytic activity. In a certain way, these results are surprising since the mechanism of photoinduced electron transfer and photosensitization generally requires a close contact between the species in the electronically excited state and the electron-transfer quencher and this situation requires, probably, prior encapsulation of the dye. In fact, optimization of the MOFs containing adsorbed RhB by washing RhB/Pt@UiO-66(Zr)-100 to remove the excessive adsorbed dyes, results in the highest photocatalytic activity with a rate of 116 μmol g^{-1} h^{-1}, which is 30-fold greater than that of bare Pt@UiO-66(Zr). Moreover, comparable photoactivity was achieved when the same amount of RhB (11.92 mg g^{-1}) was directly added to the solution. Therefore, the photocatalytic

activity of both UiO-66(Zr) and Pt@UiO-66(Zr) were not positively correlated to the amounts of dye adsorbed, a fact that certainly deserves further study to determine the quenching mechanism of RhB excited sates by UiO-66 particles. Powder XRD patterns of the fresh and used RhB-sensitized Pt@UiO-66(Zr) are identical implying that Pt@UiO-66(Zr) is resistant to light irradiation. The photostability of Pt@UiO-66(Zr) was also investigated over three runs of 15 h in total. Another point to consider is, however, the photostability of RhB dye in the process. Further research should be aimed at anchoring a suitable dye sensitizer onto the porous MOFs to enhance overall photocatalytic activity.

Recently, Erythrosin B (ErB, see structure in Figure 13) dye-sensitized UiO-66 octahedra has been reported for the

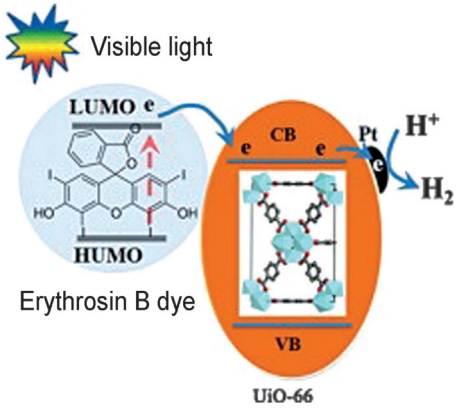

Figure 13. Pictorial illustration of ErB photosensitization of UiO-66 containing Pt (reproduced with permission from Ref. [86]).

photocatalytic H_2 production.[86] The pristine Pt-UiO-66 (0.5 wt% Pt) catalyst showed no activity for H_2 production due to the lack of visible-light absorption. Also, trace amounts of H_2 evolution were detected from ErB dye suspension (5 mg) in the presence of H_2PtCl_6 solution. Among the various catalysts examined, a maximum of H_2 evolution was achieved with Pt-UiO-66-30 (the number 30 indicates the amount of ErB dye) to around 37 μmol.[86] After three cycles of photoreactions, the H_2 production activity still retains over 80%, suggesting the photostability of ErB and Pt-UiO-66 for H_2 generation system, but however, leaching or instability of ErB could not be avoided. Furthermore, traces of Zr^{4+} ions were also detected by ICP-AES analysis of the aqueous solution. Dye decomposition is the general drawback of this approach that should be convincingly addressed.

In the last two studies, the dyes were present in the suspension, but not incorporated into the MOF lattice. The flexibility that MOFs offer in the selection of the building block for their synthesis as well as the large variety of strategies for post-synthetic modification allows MOFs to be prepared in which the chromophore forms part of the structure. In this regard, a Ti-based MOF [Ti-MOF-Ru(tpy)$_2$] incorporating a bis(4′-(4-carboxyphenyl)-terpyridine)Ru^{II} complex [Ru(tpy)$_2$] (Scheme 6) as organic linker and light harvesters has been prepared. The photocatalytic activity of Ti-MOF-Ru(tpy)$_2$ for H_2 production under visible light

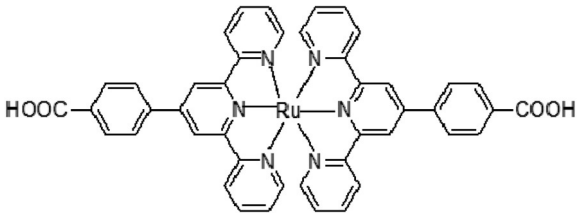

Scheme 6. Chemical structure of the Ru(tpy)$_2$ complex used as building block of Ti-MOF-Ru(tpy)$_2$.

irradiation up to 620 nm in aqueous solution containing TEOA as a sacrificial electron donor has been investigated.[87] The selection of Ru(tpy)$_2$ as the linker was based on its wide absorption band in the visible region and the lower energy of its HOMO level compared to 2-atp, as confirmed by cyclic voltammetry and diffuse-reflectance UV/Vis spectroscopy. Thus, it can be expected that the photocatalytic H_2 generation proceeds upon irradiation with long wavelength visible light using TEOA, EDTA, CH_3OH, or other compound as a sacrificial electron donor. The surface area of Ti-MOF-Ru(tpy)$_2$ was determined to be 20 $m^2 g^{-1}$, indicating that the sample is not porous. Pt/Ti-MOF-Ru(tpy)$_2$ (1 wt% Pt) exhibited steady H_2 production (5.1 μmol) under visible-light irradiation without a significant loss of photocatalytic activity over at least three cycles. Interestingly, even in the absence of Pt NPs, 2.1 μmol of H_2 is produced by Ti-MOF-Ru(tpy)$_2$. In contrast, the organic linker (Ru(tpy)$_2$) showed no photocatalytic activity under the same conditions. Furthermore, the adsorption of Ru(tpy)$_2$ on Degussa P25 TiO_2 (Ru(tpy)$_2$-TiO_2) gave no H_2 evolution and this lack of photocatalytic activity was proposed to be due to the Ru(tpy)$_2$ detachment from the TiO_2 surface under the reaction conditions, disfavoring the transfer of photogenerated electrons from excited Ru(tpy)$_2$ to CB of TiO_2. This control using Ru(tpy)$_2$-TiO_2 shows the advantage of the photocatalytic system based on MOFs, in which titanium-oxo clusters and Ru(tpy)$_2$ are rigidly immobilized. Among the various sacrificial reagents investigated, TEOA exhibit higher H_2 evolution than EDTA and CH_3OH using Ti-MOF-Ru(tpy)$_2$, but, however, NH_2-MIL-125(Ti) gave no H_2 as a photocatalyst under the same conditions. These results can be attributed to the higher oxidation power of Ru(tpy)$_2$ than that of 2-atp, although other factors, particularly the large extinction coefficient of Ru(tpy)$_2$ which ensures more efficient light harvesting and longer lifetime of the excited state in the triplet manifold can play a crucial role on the overall efficiency of the photocatalytic process. Powder XRD of Ti-MOF-Ru(tpy)$_2$ remains unaltered after the reaction indicating framework stability.

Two 3D frameworks $[Cu(en)_2]_4[PNb_{12}O_{40}(VO)_6]\cdot(OH)_5\cdot 8H_2O$ and $[Cu(enMe)_2]_4[PNb_{12}O_{40}(VO)_6]\cdot(OH)_5\cdot 6H_2O$ (enMe = 1,2-diaminopropane) were obtained and their photocatalytic activities were tested for H_2 production (Figure 14).[88] Both MOFs $[Cu(en)_2]_4[PNb_{12}O_{40}(VO)_6]\cdot(OH)_5\cdot 8H_2O$ and $[Cu(enMe)_2]_4[PNb_{12}O_{40}(VO)_6]\cdot(OH)_5\cdot 6H_2O$ contain the hexa-capped Keggin phosphoniobate, $[PNb_{12}O_{40}(VO)_6]^{3-}$, which was used as the building block for constructing the 3D framework materials.[88] The photocata-

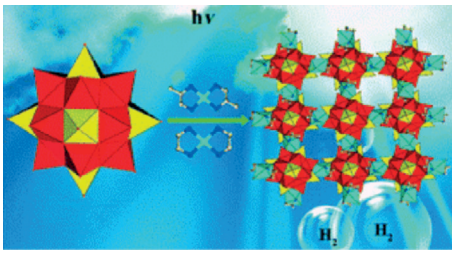

Figure 14. Schematic illustration of the Keggin phosphoniobate as a building block and the two 3D photocatalytic MOFs that may result from it (reproduced with permission from Ref. [88]).

lytic H_2 evolution activity of $[Cu(en)_2]_4[PNb_{12}O_{40}(VO)_6]\cdot(OH)_5\cdot 8H_2O$ (100 mg) was investigated using 0.75 wt% Pt as the co-catalyst in 20% aqueous CH_3OH solution (100 mL). The continuous evolution of H_2 at a rate of 44.35 μmol g^{-1} h^{-1} was observed, reaching a total amount of H_2 of 33.26 μmol in 7.5 h under the UV irradiation (125 W Hg lamp), with a TON of 1.05. On the other hand, MOF $[Cu(en)_2]_4[PNb_{12}O_{40}(VO)_6]\cdot(OH)_5\cdot 8H_2O$ exhibited a continuous H_2 evolution at a rate of 43.86 μmol g^{-1} h^{-1} and 10.45 μmol g^{-1} h^{-1} under Hg and Xe lamp irradiation, respectively. Both MOFs showed no significant changes in the powder XRD after the photocatalytic experiments indicating their photostability.

In a different approach, MOFs have been used as precursors of photocatalysts. In one of these examples, Fe-containing MIL-101(Fe) nanometric MOF was coated with amorphous titania followed by calcination to produce crystalline $Fe_2O_3@TiO_2$ composite NPs (Figure 15). The photocatalytic activity of this core–shell nanocomposite was investigated in H_2 production from H_2O under visible light.[89] The amorphous titania shell was estimated to be 1.2 nm thick, assuming it forms a continuous shell on the Fe_2O_3 particles derived from MIL-101(Fe) calcination. During the preparation of this composite, although powder XRD indicated some

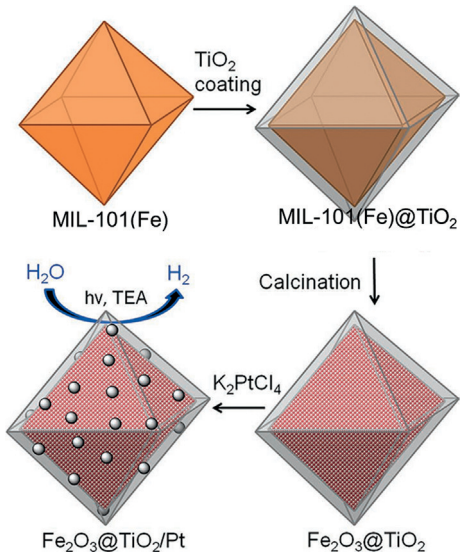

Figure 15. Illustration of the preparation method of $Fe_2O_3@TiO_2$/Pt core@shell NPs using MIL-101(Fe) as a precursor of the Fe_2O_3 core (reproduced from permission from Ref. [89]).

loss of crystallinity, the peaks corresponding to MIL-101(Fe) still appear for the coated particles, indicating that MIL-101(Fe) does not decompose under the conditions required for the preparation of the TiO_2 coating. Furthermore, the peaks corresponding to TiO_2 did not appear in the powder XRD pattern for the core–shell particles, indicating that the titania shell prepared in the coating step was amorphous. In total contrast, after calcination the nanocomposite is composed of a shell of anatase phase TiO_2 and the core of hematite phase Fe_2O_3 (α-Fe_2O_3) as indicated by powder XRD. The amount of Fe and Ti was determined by ICP-MS analyses for calcined particles corresponding to 80 wt% of Fe_2O_3 and 20 wt% of TiO_2. TEM images did not allow distinguishing between the TiO_2 and Fe_2O_3 regions. The BET surface area was found to be 11.6 m^2 g^{-1} for $Fe_2O_3@TiO_2$. TiO_2 is highly active photocatalyst[113] in the UV, while Fe_2O_3 absorbs visible light, but its CB is not at high enough potential to drive H_2 generation. The photocatalytic activity for H_2 generation of the $Fe_2O_3@TiO_2$ material was studied in combination with K_2PtCl_4 added to the solution to form, by photodeposition, homogeneously dispersed Pt NPs (2–4 nm) at the initial stage of the reaction. The evolution of H_2 increased linearly during irradiation, reaching a total of 30 μmol H_2 per mg of material using TEA as a sacrificial electron donor after 48 h. $Fe_2O_3@TiO_2$/Pt showed no appreciable change in its efficiency during the second or third cycles. While powder XRD of the material remains unchanged showing the same crystalline phases, TEM images of the recovered material revealed that many of the outer shells break apart, indicating that the $Fe_2O_3@TiO_2$/Pt photocatalyst is not stable during the generation of H_2.

Owing to the large pore volume of MOFs, they can, like zeolites, also play a passive role incorporating photocatalytically relevant components. In one example of this strategy, MIL-101(Cr) has been used because of its high resistance to air, H_2O, common solvents, and thermal treatment.[111,114] For this reason MIL-101(Cr) is a suitable MOF to be used in an aqueous medium. Thus, Pt@CdS/MIL-101(Cr) (0.5 wt% Pt) has been reported as a photocatalyst for H_2 production in lactic acid aqueous solution under visible-light ($\lambda > 420$ nm) irradiation.[90] In contrast, no appreciable H_2 evolution was detected over MIL-101(Cr) in the absence of CdS, indicating that MIL-101(Cr) is not an effective photocatalyst by itself. On the other hand, TEM images of Pt@CdS/MIL-101(Cr) after in situ photoreduction of Pt showed many small Pt NPs deposited on the CdS surface but not on MIL-101(Cr). The rate of H_2 evolution depends on CdS loading. The maximum H_2 evolution of 150 μmol h^{-1} was achieved with 10 wt% CdS. Under the optimized reaction conditions, the H_2 production rate increased in the following order: CdS mixed MIL-101(Cr) < bare CdS < CdS/MIL-101(Cr)(10 wt%). The photostability of CdS/MIL-101(Cr)(10 wt%) was investigated over four consecutive runs without noticeable changes in H_2 evolution and the long-term durability of the catalysts was also satisfactory. Powder XRD patterns of the fresh and used CdS/MIL-101(Cr) (10 wt%) were almost identical implying that the material is stable during the photocatalytic reaction. The importance of the selection of a robust MOF[115] was clearly demonstrated by preparing an analogous material in

which CdS was incorporated in MOF-5. The resulting CdS/MOF-5 exhibited negligible activity for the photocatalytic H_2 evolution under the same experimental conditions. The poor photocatalytic activity of CdS/MOF-5 may be explained as a consequence of the lack of MOF-5 stability and the collapse of the framework after CdS incorporation. In comparison with MIL-101(Cr) and MOF-5, MCM-41 showed decreased H_2 production compared to bare CdS although it possesses a mesoporous structure with a considerable specific surface area. This result shows the superior performance of MOF-based materials compared to mesoporous materials, but the origin of this superior performance deserves deeper study and understanding.

In a similar type of strategy, the ternary composite UiO-66/CdS/rGO (rGO = reduced graphene oxide) has been designed and its photocatalytic activity for H_2 production under visible light using 1 wt% Pt was studied (Figure 16).[91]

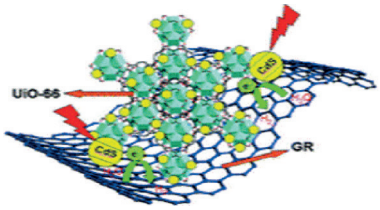

Figure 16. Schematic representation of the composition and the operation mechanism of a ternary photocatalytic system comprising CdS quantum dots as a visible-light semiconductor, UiO-66 and rGO to accept photogenerated electrons, increasing the efficiency of the process (reproduced with permission from Ref. [91]).

The use of graphene oxide (GO) and other types of graphene to enhance the photocatalytic activity of semiconductors by favoring charge separation has been recently well documented by a large number of examples.[116–120] In this regard, the combination of the properties of MOFs and rGO could also be beneficial. The photocatalytic activity of UiO-66/CdS/rGO was compared with CdS over an inorganic semiconductor, such as P25/CdS/1 %rGO. The H_2 production rate was 13.8 (105 μmol h^{-1}) and 11.2 mmol g_{CdS}^{-1} h^{-1} for UiO-66/CdS/1 %rGO and UiO-66/CdS, respectively. On the other hand, P25/CdS/1 %rGO resulted in 7 mmol g_{CdS}^{-1} h^{-1}. The H_2 generation rate of CdS modified with both UiO-66 and rGO was about 13.8 times as high as that of non-modified CdS.

The influence of different amounts of rGO on H_2 production activity was also studied and the best result achieved with 1 wt% rGO in the ternary hybrid. Of all the composites this value of 1 wt% is in-line with the percentages commonly reported for optimized photocatalytic composites containing GO.[121] The enhanced activity of UiO-66/CdS/1 %rGO may be attributed to its higher BET specific surface area (705 $m^2 g^{-1}$) with respect to P25/CdS/1 %rGO (62 $m^2 g^{-1}$). Furthermore, TEM images show that CdS was distributed more homogeneously on UiO-66 than on P25, and CdS supported on P25 is more inclined to agglomerate. UiO-66 with its larger specific surface area should allow a better dispersion of CdS compared to P25. Photocurrent measurements were used to study the interface charge separation efficiency, since higher photocurrent intensity is often associated with better photocatalytic activity. Photocurrent spectra showed that the photocurrent intensity of UiO-66/CdS/1 %rGO was higher than that of P25/CdS/1 %rGO, which reveals enhanced interface charge-separation efficiency with UiO-66 than for P25, in good agreement with the photocatalytic tests. Thus, enhancement of H_2 evolution activity observed for UiO-66/CdS/1 %rGO is largely derived from the combination of the favorable properties of MOF and rGO, resulting in increasing the surface area and minimizing the recombination of charge carriers. The XRD pattern showed that the UiO-66 structure remained unchanged during the reaction.

Matsuoka and co-workers have prepared an NH_2-functionalized Ti^{IV}-MOF NH_2-MIL-125(Ti) that contains 2-atp instead of the bdc present in the parent compound (MIL-125). TiO_2 is the most studied photocatalyst and nanometric clusters of Ti_xO_y have also been reported to exhibit a high photocatalytic activity under UV irradiation.[122] As commented in the previous Sections, the presence of -NH_2 groups in the linker introduces an additional absorption band in the MOF that makes possible visible-light excitation. The photocatalytic activity of NH_2-MIL-125(Ti) was probed for the photocatalytic H_2 production reaction using TEOA as a sacrificial electron donor.[92] Upon irradiation ($\lambda >$ 420 nm), continuous H_2 production was observed from the beginning of the irradiation period, and the total evolution of H_2 reaches to 33 μmol after 9 h showing that Pt/NH_2-MIL-125(Ti) acts as a visible-light-responsive photocatalyst. Pt/NH_2-MIL-125(Ti) did not lose its photocatalytic activity over three cycles and the recovered photocatalyst exhibited a slightly lower BET surface area (742 $m^2 g^{-1}$) and a marginal decrease in the intensities of the diffraction peaks of the MIL-125(Ti) structure, indicating that the porous network has partially deteriorated, although this degree of crystallinity loss has only a small impact on the photocatalytic activity. In contrast, Pt/MIL-125(Ti) displays no photocatalytic activity under visible-light irradiation. This indicates that visible-light photoresponse is associated with the 2-atp moiety. The probable photophysical mechanism starts with the organic linker 2-atp absorbing the incident visible light and its excited state injects electrons to CB of octameric titanium-oxo clusters in the manner expected for a linker-to-cluster single-electron-transfer mechanism. As it could be anticipated, NH_2-MIL-125(Ti) (5 μmol H_2) exhibited a lower photocatalytic activity than Pt/NH_2-MIL-125(Ti) (10 μmol H_2) after 3 h, in agreement with the expected role of Pt NPs as co-catalysts enhancing the efficiency of H_2 evolution. Interestingly, Pt/NH_2-MIL-125(Ti) did not promote H_2 with other sacrificial electron donors, such as TEA, EDTA, and CH_3OH. This failure was attributed to the weak oxidation power of the organic 2-atp linker. However, this proposal should be confirmed in view of the similar reduction power expected for TEOA and TEA. The selectivity on the photocatalytic H_2 evolution as a function of the sacrificial electron donor is very rare and could be exploited to gain selectivity in various photocatalytic processes. Generally photocatalysis has a lack of selectivity and does not distinguish between electron donors, a result of the high oxidation potential of photo-

generated holes in most semiconductors. On the other hand, Pt/NH_2-MIL-125(Ti) showed a much higher H_2 evolution rate (11.7 μmol h^{-1}) under UV light ($\lambda > 300$ nm) irradiation probably as consequence of the direct excitation of titanium-oxo clusters.

NH_2-MIL-125(Ti) with different loading amounts of Pt as a co-catalyst has been prepared by photodeposition and its photoactivity for the H_2 production investigated using 0.01 M aqueous TEOA solution under visible light ($\lambda > 420$ nm) irradiation at room temperature.[93] XAFS measurements revealed that the deposited Pt on NH_2-MIL-125(Ti) exist as mixed states of metal and ion. One of the possible advantages of using porous solids to incorporate Pt NPs could be the small particle size of the NPs which is limited by the dimensions of the pores. Accordingly, TEM images did not show the presence of Pt NPs for Pt loadings up to 2 wt % and this failure was attributed to the small particle size. Under the optimized reaction conditions, the evolution of H_2 increased upon increasing the Pt loading, achieving a maximum of 15.5 μmol for 1.5 wt % of Pt loading in 3 h using visible-light irradiation. In agreement with the current ideas concerning the influence of Pt NPs[123] on the photocatalytic activity of semiconductors, it was proposed that Pt co-catalysts accelerate the H_2 production reactions by trapping the photogenerated electrons, inducing efficient charge separation. The time course of photocatalytic H_2 production under visible-light irradiation over Pt(1.5)/NH_2-MIL-125(Ti) for a total of 9 h with intermittent evacuation and exposure to atmospheric conditions every 3 h indicated no significant loss of photocatalytic activity and this test was considered as a proof of the photostability of Pt/NH_2-MIL-125(Ti). Certainly, much longer exposure times are necessary to convincingly demonstrate the complete photostability of this MOF. In contrast, Pt/MIL-125(Ti) showed no photocatalytic activity under identical conditions, illustrating again the role of -NH_2 substituents as promoters of visible light photoresponse. In situ ESR measurements provide evidence supporting that the reaction proceeds through photoinduced electron transfer from the organic linker to the deposited Pt as a co-catalyst by way of titanium-oxo clusters.

It is clear that the preparation procedure of the photocatalyst and, particularly, how Pt NPs are formed and their location and size should strongly influence the photocatalytic activity of the resulting MOF. Thus, recently, a facile and general methodology has been reported for the fabrication of highly dispersed Au, Pd, and Pt NPs on MIL-125(Ti) without using reducing and capping agents.[94] Noble metal NPs formation is directed by an in situ redox reaction between the reductive MIL-125(Ti) with Ti^{3+} and oxidative metal salt precursors (Scheme 7). The photocatalytic activity of these composites was evaluated in H_2 evolution in aqueous solution containing TEOA as a sacrificial agent. TEM images revealed that the average diameters of Pt NPs are 3 nm. The total production of H_2 achieved using Pt/MIL-125(Ti) is 38.68 μmol after 5 h irradiation.[94] MIL-125(Ti) without Pt deposition exhibited very low photoactivity in H_2 generation. It is worth mentioning that Pt/MIL-125(Ti) obtained through this Ti^{3+}-assisted method showed superior activity compared to the sample Pt/MIL-125(Ti)-PD prepared via a direct photodeposition (PD) method. Thus, the corresponding TON based on the Pt is 30.2 for the sample prepared using Ti^{3+} reduction, which is about 80 % higher than the activity of Pt/MIL-125(Ti)-PD. This enhanced activity could be ascribed to the fact that the incorporation of noble metals into MIL-125(Ti) might form a Schottky barrier and the photoelectrons can easily be transferred from MIL-125(Ti) which has a low work function to Au, Pd, and Pt NPs which have high work functions because of their intimate interfacial contact and adequate location within the MOF crystal, which significantly should enhance the separation and lifetime of photogenerated carriers.

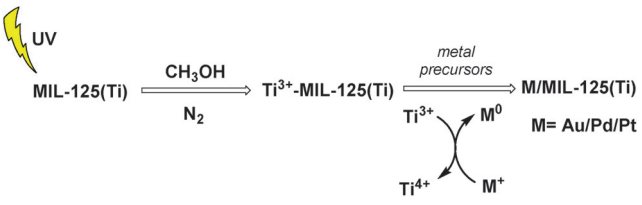

Scheme 7. Preparation of metal NPs on MIL-125(Ti).

Very recently, cobaloxime-derived NH_2-MIL-125(Ti) Co@NH_2-MIL-125(Ti) MOF-based composite has been reported to exhibit light-driven H_2 production.[95] Co@NH_2-MIL-125(Ti) was synthesized by adsorbing the flexible organic ligand $LH_2(DOH)_2$pn onto the pores of NH_2-MIL-125(Ti), followed by the addition of $CoBr_2$ under aerobic conditions to assemble the cobaloxime complex within the large cavities of NH_2-MIL-125(Ti) (Scheme 8). ICP analysis confirmed the presence of cobalt-containing species in the MOF, with the total cobalt content ranging between 1.1–2.7 wt %. The pristine NH_2-MIL-125(Ti) had a total pore volume of 0.58 $cm^3 g^{-1}$ whereas the Co@NH_2-MIL-125(Ti) has a total pore volume of 0.46 $cm^3 g^{-1}$. Furthermore, the pristine MOF consists of well-defined crystallites with a diameter of approximately 400 nm. On the other hand, Co@NH_2-MIL-125(Ti) crystallites are nearly identical to the parent MOF with no agglomerates or core/shell type structure, as evidenced by TEM. Also, the UV/Vis spectrum of Co@NH_2-MIL-125(Ti) exhibited two new absorption bands at 440 and 585 nm compared to the pristine framework, which are ascribed to the inclusion of the cobaloxime complex. The

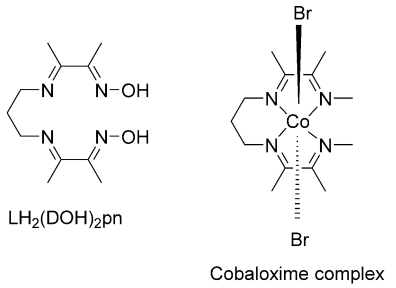

Scheme 8. Chemical structures of the $LH_2(DOH)_2$pn ligand and cobaloxime complex.

photocatalytic experiments for the generation of H_2 was assessed by suspending Co@NH_2-MIL-125(Ti) in a mixture of acetonitrile, triethylamine, and water (5:1:0.1 *v*/*v*) under visible-light illumination. Cobaloxime is known to be an electrocatalyst and it cannot act as a photocatalyst in the absence of a photosensitizer. As a consequence, no H_2 evolution is observed with cobaloxime as a homogeneous photocatalyst. Pristine NH_2-MIL-125(Ti) produced a moderate amount of H_2 (ca. 2 μmol after 20 h), while Co@NH_2-MIL-125(Ti) (ca. 37 μmol after 20 h) gave up to a 20-fold enhancement in the photocatalytic performance. Interestingly, Co@NH_2-MIL-125(Ti) maintains a constant TOF of 0.8 h^{-1} even after 65 h of total operation, indicating a high stability under illumination conditions. Moreover, similar TOFs (per Co atom) were achieved for catalysts bearing different amounts of cobalt entities, even for catalysts containing up to one cobalt atom per MOF cavity, demonstrating the absence of diffusion limitations and efficient charge transfer even at relatively high loadings. The stability of Co@NH_2-MIL-125(Ti) under the experimental conditions was confirmed by determining the absence of Co leaching and the reusability of the materials several times without loss of activity. It has to be noted that the advantage of Co@NH_2-MIL-125(Ti) as a visible-light photocatalyst for H_2 generation is that the presence of cobaloxime acting as the co-catalyst makes the presence of noble metals unnecessary, while still reaching moderate efficiencies compared with state-of-the-art semiconductor-based systems.[124,125] These activity data clearly leave room for further developments of new and modified MOFs for better photocatalytic activity.

9. Photoreduction of CO_2

The capture and efficient use of CO_2 could be a viable strategy to decrease the amounts of CO_2 released to the atmosphere by burning fossil fuels. Decrease of CO_2 emissions to the atmosphere is considered crucial to avoid global warming. One of the possibilities that are attracting increasing interest is to convert CO_2 into fuels by means of solar energy.[23,126–128] Thus, many research efforts have been focused on the development of efficient heterogeneous photocatalysts for the solar-light-induced reduction of CO_2. One of the long term goals is to develop artificial photosynthesis for the conversion of CO_2 and H_2O into chemicals.

NH_2-MIL-125(Ti) has been reported as a photoactive catalyst for the reduction of CO_2 under visible-light irradiation.[96] Both NH_2-MIL-125(Ti) and NH_2-UiO-66[83] present an extra absorption band in the visible region around 450 nm, which is responsible of the bright yellow color of these solids. Besides light harvesting, another general beneficial role of -NH_2 is to increase CO_2 adsorption on the MOF by providing some weak basic sites to interact with acidic CO_2. It was observed that the maximum CO_2 uptake for NH_2-MIL-125(Ti) and parent MIL-125(Ti) were 132.2 and 98.6 $cm^3 g^{-1}$, respectively. The photocatalytic reduction of CO_2 was performed in CH_3CN with TEOA as a sacrificial agent under visible-light irradiation. A temporal concentration change of $HCOO^-$ as a function of irradiation time in the presence of NH_2-MIL-125(Ti) showed that the amount of $HCOO^-$ reaches to 8.14 μmol in 10 h. Physicochemical characterization by XRD, BET, and TGA, as well as IR and Raman spectra of NH_2-MIL-125(Ti) after the photocatalytic reaction showed that NH_2-MIL-125(Ti) remains stable during the photocatalytic CO_2 reduction. Furthermore, when the photocatalytic study was carried out using benzyl alcohol as an electron donor, upon visible-light irradiation no $HCOO^-$ is detected. Apparently, in addition to acting as an electron donor, TEOA can facilitate the photocatalytic CO_2 reduction because of its more basic nature allowing adsorption of CO_2. On the other hand, the photocatalytic reduction of CO_2 over NH_2-MIL-125(Ti) exhibited higher activity than the parent MIL-125(Ti) under 365 nm UV irradiation, a fact attributable to its higher CO_2 uptake compared to MIL-125(Ti). Isotopic labelling experiment using $^{13}CO_2$ confirms that the formation of $HCOO^-$ originates from CO_2 and not from any adventitious organic adsorbate that can be present on the MOF. One likely possibility that has always to be addressed and ruled out is the linker being the source of some $HCOO^-$ as a result of photochemical degradation, rather than CO_2 reduction. Firm evidence of CO_2 reduction is isotopic labelling to confirm the formation of 100% $H^{13}COO^-$ from $^{13}CO_2$ reduction. Although the activity for the reduction of CO_2 with the current NH_2-MIL-125(Ti) catalyst is still low, considering the versatility that MOFs offer in terms of coordination chemistry of the metal cations, the availability of different organic linkers, and the possibility to modulate the composition, structure, and properties of the MOFs, these results provide a proof of concept for future development of the field aimed at the synthesis of highly efficient MOF-based photocatalysts for the reduction of CO_2.

Metal NPs doped over NH_2-MIL-125(Ti) (M = Pt and Au) were prepared and their effect on the photocatalytic performance of NH_2-MIL-125(Ti) has been studied in saturated CO_2 with TEOA as a sacrificial agent under visible-light irradiation.[97] The size of the Pt clusters was estimated to be about 30 Å in Pt/NH_2-MIL-125(Ti) while the size of Au NPs was estimated to be about 25 Å in Au/NH_2-MIL-125(Ti). Deposition of Pt and Au in NH_2-MIL-125(Ti) resulted in the decrease of CO_2 adsorption from 132.2 for parent NH_2-MIL-125(Ti) to 90.2 for Pt/NH_2-MIL-125(Ti) and 117.4 $cm^3 g^{-1}$ for Au/NH_2-MIL-125(Ti). The photocatalytic activity of these MOFs was tested for CO_2 reduction. The $HCOO^-$ production rate using pure NH_2-MIL-125(Ti) was 10.75 μmol after 8 h. In contrast, Au/NH_2-MIL-125(Ti) exhibited 9.06 μmol of $HCOO^-$ at 8 h, which is lower by 16% compared to pure NH_2-MIL-125(Ti). However, Pt/NH_2-MIL-125(Ti) showed an unusual enhancement in the production of $HCOO^-$ after 8 h to the value of 12.96 μmol, about 21% increase in the activity as compared to pure NH_2-MIL-125(Ti). It was noticed that the amount of $HCOO^-$ increases almost linearly with the irradiation time over both metal-doped NH_2-MIL-125(Ti) MOFs. This suggests that both metal-doped NH_2-MIL-125(Ti) MOFs are stable during the photocatalytic reactions and the lower amount of $HCOO^-$ observed using Au/NH_2-MIL-125(Ti) is not due to photocatalyst deactivation. This influence of the presence of metal co-catalyst is however, very minor in absolute terms and surely does not justify the use of

costly noble metals. Concerning the reaction mechanism, it is proposed that $HCOO^-$ should be derived from the reaction of evolved H_2 with CO_2. As it has been reported that Ti^{3+} generated by the reduction of Ti^{4+} is the active species responsible for photocatalytic $HCOO^-$ production using NH_2-MIL-125(Ti),[96] and H_2 is a good reducing agent, it is speculated that H_2 formed photocatalytically over M/NH_2-MIL-125(Ti) could be involved in the photocatalytic $HCOO^-$ production, especially under the assistance of the noble metal NPs, which should promote the dissociation and the activation of H_2. This hypothesis was supported by ESR spectroscopy and may account for the different activity of Pt- and Au-loaded NH_2-MIL-125(Ti). However, it should be noted that the solubility of H_2 in H_2O is always low, regardless the pH value, and this mechanism would require the build-up of a high H_2 concentration in the photoreactor that should have been detected and quantified since it would have provided a valuable information.

Recently, a series of Fe-containing MOFs namely, MIL-101(Fe), MIL-53(Fe), and MIL-88B(Fe) has been reported as photocatalysts for CO_2 reduction to give $HCOO^-$.[100] Among the three investigated Fe-based MOFs, MIL-101(Fe) showed the best activity, a fact that was attributed to the existence of unsaturated coordination positions around Fe ions in its structure. This enhanced activity is due to the direct excitation of the Fe–O clusters in these MOFs that induces an electron transfer from O^{2-} to Fe^{3+} to form Fe^{2+}, which is responsible for the photocatalytic CO_2 reduction. The activity of these Fe-MOFs was compared with their respective NH_2-substituted MOFs under visible-light irradiation. As expected, all three NH_2-functionalized Fe-containing MOFs (NH_2-MIL-101(Fe), NH_2-MIL-53(Fe), and NH_2-MIL-88B(Fe)) showed enhanced photocatalytic activity (Table 2) in comparison to the non-functionalized MOFs, owing to the existence of dual excitation pathways, that is, excitation of the NH_2-substituted linker followed by an electron transfer to the Fe center in addition to the direct excitation of Fe–O clusters.

Table 2: The photocatalytic activity of Fe-containing MOFs and of their respective NH_2-functionalized MOFs in CO_2 reduction after 8 h.[a]

Photocatalyst	$HCOO^-$ [μmol]
NH_2-MIL-101(Fe)	178.0
MIL-101(Fe)	59.0
NH_2-MIL-53(Fe)	46.5
MIL-53(Fe)	29.7
NH_2-MIL-88(Fe)	30.0
MIL-88(Fe)	9.0

[a] Data is taken from Ref. [100].

The large flexibility that MOFs offer in synthesis and design is again exemplified by the possibility to prepare MOFs having more than one linker ("mixed-ligand MOFs") or/and more than one metal ("mixed-metal MOFs"). In this regard, the photocatalytic activity of NH_2-UiO-66(Zr) can be improved for the photoreduction of CO_2 under visible-light irradiation incorporating 2,5-diaminoterephthalate (dta) in the structure. The photocatalytic activity of dta-modified NH_2-UiO-66(Zr), NH_2-UiO-66(Zr) was evaluated using TEOA as a sacrificial agent (Scheme 9).[98] Compared to pure 2-atp, the absorption maximum of the resultant mixed-ligand 2-atp-dta NH_2-UiO-66(Zr) is shifted to the short wavelength region, which can be ascribed to the interaction between the ligand and the Zr–O clusters. On the other hand, the presence of -NH_2 groups has influence on the CO_2 adsorption capacity of the MOF. Thus, NH_2-UiO-66(Zr) showed a higher adsorption capability toward CO_2 than its parent UiO-66(Zr). At 1 atm and 273 K, the maximum CO_2 uptake for NH_2-UiO-66(Zr) was 68 $cm^3 g^{-1}$, whereas for UiO-66(Zr) is 53 $cm^3 g^{-1}$. The concentration of $HCOO^-$ over NH_2-UiO-66(Zr) increases with the irradiation time, reaching 13.2 μmol after 10 h. This value is higher than that achieved over other related photoactive NH_2-MIL-125(Ti) MOFs (8.14 μmol) under similar reaction conditions. The photo-induced electron transfer from the excited 2-atp to the Zr-oxo clusters in NH_2-UiO-66(Zr) to generate Zr^{III} was proposed to be responsible for the enhanced activity based on photoluminescence studies. It has to be, however, commented that conclusions on the relative activity of different photocatalysts based on data obtained from different laboratories have to be taken cautiously. Light intensity, the lamp emission spectrum, reaction temperature, and particularly, photoreactor design, and deposition of the photocatalyst are all experimental parameters of crucial importance with respect to the observed efficiency of the photocatalytic reaction that are difficult to reproduce from different laboratories. This difficulty in obtaining absolute activity data in photocatalysis is a significant limitation that has complicated the progress in this area. The stability of NH_2-UiO-66(Zr) was evaluated by measuring XRD, IR spectra, and BET surface area before and after the photocatalytic reduction of CO_2, wherein no significant changes were observed. A prolonged photocatalytic reaction revealed that the production of $HCOO^-$ increases steadily to 25 μmol after 24 h, and this linear evolution of $HCOO^-$ with time further confirms the stability of NH_2-UiO-66(Zr) in the photocatalytic CO_2 reduction. Reusability data of the photocatalyst for multiple cycles or until catalyst deactivation would have thrown some valuable insights on the catalyst stability. The photocatalytic reduction of CO_2 using mixed-ligand 2-atp-dta NH_2-UiO-66(Zr) gave 20.7 μmol of $HCOO^-$ after 10 h, which is more than 50% higher compared with single 2-atp ligand NH_2-UiO-66(Zr) (13.2 μmol) under identical conditions. This higher photocatalytic activity of the mixed-ligand MOF is attributable to its high light absorption and increased CO_2 adsorption owing to the presence of additional -NH_2 groups in mixed-ligand NH_2-UiO-66(Zr). On

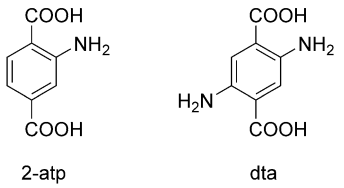

Scheme 9. Chemical structures of 2-atp and dta used as ligands to construct UiO-66.

the other hand, photocatalytic reactions with wavelength longer than 515 nm gave 7.28 μmol of $HCOO^-$ over mixed-ligand NH_2-UiO-66(Zr), while no $HCOO^-$ is formed over NH_2-UiO-66(Zr) upon illumination in this spectral region. These photocatalytic data support that additional light absorption introduced by the second -NH_2 group in the mixed-ligand NH_2-UiO-66(Zr) is responsible for the enhanced photocatalytic performance.

The photocatalytic activity for H_2 generation of a mixed-metal MOF NH_2-UiO-66(Zr/Ti) has already been commented in the previous Section. Not surprisingly, the photocatalytic activity of the most active NH_2-UiO-66(Zr/Ti)-120-16 sample was also tested as photocatalyst for CO_2 reduction. TEOA was selected as sacrificial agent in these studies,[84] which acts as both electron and H_2 donor and provides the basic environment to facilitate CO_2 adsorption. The photocatalytic CO_2 reduction was carried out under visible-light irradiation. No gaseous products, such as CO, CH_4, ethane, or H_2, were detected. It was observed that the concentration of $HCOO^-$ increased almost linearly with time and about 5.8 mmol mol^{-1} was achieved with NH_2-UiO-66(Zr/Ti)-120-16 after 10 h, which is 1.7 times that observed over NH_2-UiO-66(Zr) (3.4 mmol mol^{-1}) under identical conditions. Interestingly, the reaction performed with $^{13}CO_2$ over the MOFs confirmed that the source of $HCOO^-$ is CO_2. Powder XRD and isothermal N_2 adsorption/desorption of NH_2-UiO-66(Zr/Ti)-120-16 after reactions showed that the material is stable during the photoreduction of CO_2. A control experiment revealed that NH_2-UiO-66(Zr/Ti)-100-4, with a comparable CO_2 adsorption capability (80 $cm^3 g^{-1}$) to NH_2-UiO-66(Zr/Ti)-120-16 gave only 4.2 mmol mol^{-1} of $HCOO^-$ in a similar reaction time, which is higher than that over pristine NH_2-UiO-66(Zr), but lower than observed for NH_2-UiO-66(Zr/Ti)-120-16. The values of the photocatalytic activity of NH_2-UiO-66(Zr/Ti)-120-16 and NH_2-UiO-66(Zr/Ti)-100-4 clearly indicate that the higher CO_2 adsorption by NH_2-UiO-66(Zr/Ti)-120-16 alone does not result automatically in a the better activity. Furthermore, it indicates that in addition to CO_2 adsorption capability, factors related to how the incorporated Ti centers affect the photophysics of the material play an important role in the improvement of the photocatalytic performance of NH_2-UiO-66(Zr/Ti)-120-16. The enhanced activity shown by this catalyst in both photocatalytic CO_2 reduction and H_2 evolution was rationalized by DFT studies. These calculations indicate a favorable electron transfer from excited 2-atp to the Ti moiety to form $(Ti^{3+}/Zr^{4+})_6O_4(OH)_4$ in Ti-doped NH_2-UiO-66(Zr). However, owing to the overlap of the electronic states of Zr and Ti atoms in Ti-doped NH_2-UiO-66(Zr), Ti^{3+} can further transfer electrons to Zr^{4+} to form the photocatalytically active Zr^{3+}. Thus, it is proposed that the substituted Ti moiety may act as an electron mediator in promoting the electron transfer from 2-atp to the Zr center (Scheme 10).

Recently, a photocatalyst obtained by post-synthetic exchange through mixed-ligand, mixed-metal of UiO-66 $(Zr_{4.3}Ti_{1.7}O_4(OH)_4(C_8H_7O_4N)_{5.17}(C_8H_8O_4N_2)_{0.83}$ has been reported to be an effective photocatalyst for CO_2 photoreduction under visible-light irradiation.[99] The key reason for substituting Ti^{IV} ions in NH_2-UiO-66 is to make the SBUs

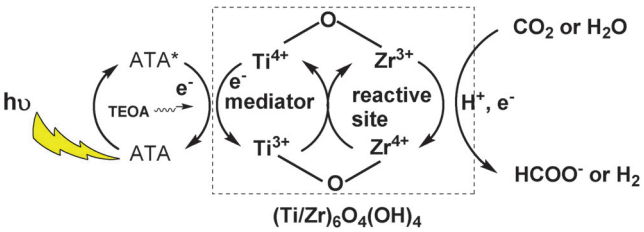

Scheme 10. A possible mechanism for the photoreduction of CO_2 by NH_2-UiO-66(Zr/Ti)-120-16, accounting for the higher photocatalytic activity of the mixed-metal MOF.

more capable of accepting electrons generated via light absorption by the organic linkers. On the other hand, introduction of a small amount of dta as a co-ligand provides new energy levels in the band structure of the MOF and favors a broader wavelength range of light absorption for the mixed-ligand MOF (Scheme 11). The ratios for Zr/Ti were 2.52 for

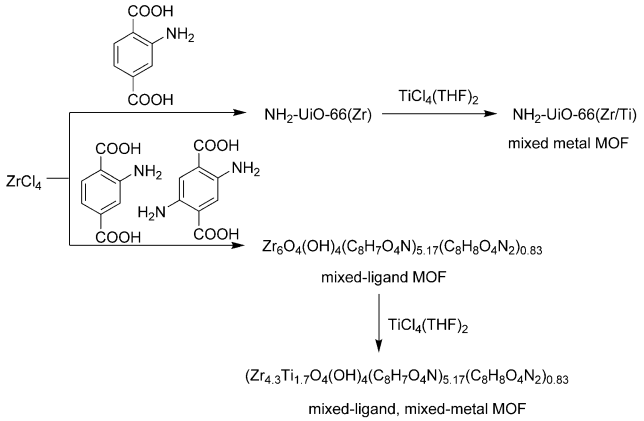

Scheme 11. Preparation of $(Zr_{4.3}Ti_{1.7}O_4(OH)_4(C_8H_7O_4N)_{5.17}$-$(C_8H_8O_4N_2)_{0.83}$ and NH_2-UiO-66(Zr/Ti) catalysts by mixed-metal and mixed-ligand strategies.

$(Zr_{4.3}Ti_{1.7}O_4(OH)_4(C_8H_7O_4N)_{5.17}(C_8H_8O_4N_2)_{0.83}$ and 3.03 for NH_2-UiO-66(Zr/Ti), respectively, as determined by ICP-MS. The photocatalytic activity of $(Zr_{4.3}Ti_{1.7}O_4(OH)_4$-$(C_8H_7O_4N)_{5.17}(C_8H_8O_4N_2)_{0.83}$ showed identical TON values over three photocatalytic cycles (6 h each), thus, indicating the catalyst stability during photocatalysis. The average TON of 6.27 ± 0.23 was observed for three independent samples. In contrast, NH_2-UiO-66(Zr/Ti) gave a lower TON (4.66 ± 0.17) than $(Zr_{4.3}Ti_{1.7}O_4(OH)_4(C_8H_7O_4N)_{5.17}(C_8H_8O_4N_2)_{0.83}$. Also, no $HCOO^-$ was detected using the parent $Zr_6O_4(OH)_4$-$(C_8H_7O_4N)_{5.17}(C_8H_8O_4N_2)_{0.83}$ and NH_2-UiO-66(Zr) catalysts, suggesting the crucial role played by Ti in the photocatalytic activity. Interestingly, photoreduction of CO_2 using NH_2-MIL-125(Ti) under the same reaction conditions resulted in a TON of 1.52 after 6 h. This value is much lower than that of $(Zr_{4.3}Ti_{1.7}O_4(OH)_4(C_8H_7O_4N)_{5.17}(C_8H_8O_4N_2)_{0.83}$ and NH_2-UiO-66(Zr/Ti). Hence, the enhanced photocatalytic activity of the mixed-metal MOF opens the door for a systematic investigation of the photocatalytic activity of cocktails of two or three different metals in MOFs.

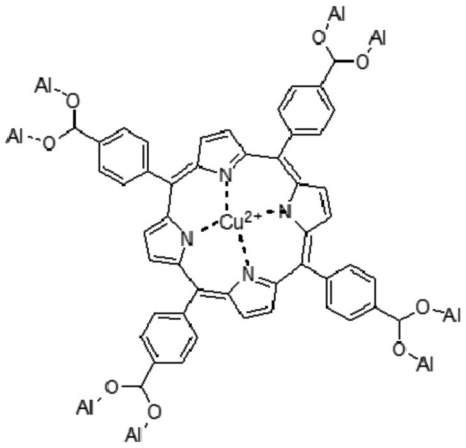

Scheme 12. Structural motif of S_{Cu} obtained by the reaction of $AlCl_3$ with S_P.

Visible-light ($\lambda \geq 420$ nm) photocatalytic CO_2 reduction in 100 mL of H_2O containing 1 mL of TEA has been reported using a Cu porphyrin (5,10,15,20-tetrakis(4-carboxyphenyl) based MOF (S_{Cu}, Scheme 12) and its activity was compared with that of an analogous MOF without Cu^{2+} (S_P).[101] Diffuse-reflectance UV/Vis spectra of S_P and S_{Cu} exhibited strong absorption from 200 to 800 nm. S_P displays a strong Soret band and four Q bands, which are characteristic for the porphyrin family. After the metallation of the porphyrin ring with Cu^{2+}, the typical four Q bands become two owing to the higher symmetry of S_{Cu}. Interestingly, S_{Cu} showed a slight red shift of the S band from 420 to 430 nm compared with S_P which is a common phenomenon for metallated porphyrins.[129] In addition, the energy-dispersive electron microscopy spectrum revealed an Al/Cu ratio of 2, indicating 100% occupancy of the porphyrin center sites by Cu^{2+}. SEM images showed that both S_{Cu} and S_P are composed of nanoplates, with a thickness of 20–30 nm. The BET surface areas were found to be 1187 and 932 $cm^2 g^{-1}$ for S_P and S_{Cu}, respectively. The CH_3OH evolution rate achieved by S_P is 37.5 ppm $g^{-1} h^{-1}$, while S_{Cu} exhibits 262.6 ppm $g^{-1} h^{-1}$, which is seven times that of S_P. The positive influence of Cu on the photocatalytic CO_2 reduction can be attributed to a more favorable CO_2 adsorption on S_{Cu} compared to S_P as evidenced by FT-IR spectroscopy. This enhanced CO_2 adsorption seems to result in higher photoreduction efficiency. Negligible CH_3OH was detected when the reaction was performed under an N_2 atmosphere instead of CO_2, upon visible-light irradiation without photocatalysts, and in the presence of photocatalyst without visible-light irradiation. Observation of CH_3OH as the product of CO_2 reduction is remarkable and, certainly, deserves further mechanistic studies to understand the origin of this selectivity. One control experiment in which $HCOO^-$ is treated under the same conditions would be important to assess the possibility of occurrence of a complete $HCOO^-$ reduction. It should be, however, commented that given the higher reactivity of CH_3OH compared to CO_2, it is unlikely that high concentration of this alcohol could be reached under photocatalytic conditions without promoting simultaneously its decomposition. Thus, at best, a steady CH_3OH concentration could be reached under these batch conditions.

MOFs can be prepared using derivatives of molecular (photo)catalysts as linkers. In this context, Ru carbonyl complexes containing bpy ligands are well-known as homogeneous catalyst for CO_2 reduction.[130] The behavior of discrete molecular complexes inspired modification of MOF-253 to incorporate Ru carbonyl complex, giving MOF-253-$Ru(CO)_2Cl_2$ that was tested as photocatalyst for CO_2 reduction under visible-light irradiation in a mixture of MeCN/TEOA (10/1).[102] ICP-OES analysis revealed that the Ru/Al ratio in MOF-253-$Ru(CO)_2Cl_2$ was 6.3%, a little lower than the theoretical Ru/Al atomic ratio of the reaction system (Ru/Al 10%). Formation of 0.67 μmol $HCOO^-$, 1.86 μmol CO, and 0.09 μmol H_2 after 8 h irradiation using MOF-253-$Ru(CO)_2Cl_2$ as a photocatalyst was observed under the optimized reaction conditions. The calculated TON for the formation of $HCOO^-$, CO, and H_2 was 2.9, 7.1, and 0.4, respectively. No products were detected using the parent MOF-253 as photocatalyst or MOF-253-$Ru(CO)_2Cl_2$ without light irradiation, indicating that the formation of the products is truly derived from photocatalysis over MOF-253-$Ru(CO)_2Cl_2$. On the other hand, the photocatalytic CO_2 reduction over the homogeneous Ru(5,5′-dcbpy)$(CO)_2Cl_2$ leads to only 0.06 μmol $HCOO^-$, 1.27 μmol CO, and 0.12 μmol H_2 under similar conditions, significantly lower values than for the heterogeneous catalyst. The better performance of MOF-253-$Ru(CO)_2Cl_2$ illustrates again the beneficial influence of immobilization of the chromophore in a rigid framework so as to avoid deactivation pathways that require mobility of the photoactive complex. The powder XRD pattern of MOF-253-$Ru(CO)_2Cl_2$ did not show any change after the reaction, thus, confirming the stability of the photocatalyst in photocatalytic CO_2 reduction. In a further improvement, $Ru(bpy)_2Cl_2$ was used to prepare a photosensitized MOF-253-$Ru(CO)_2Cl_2$. The $Ru(bpy)_2Cl_2$ can react with the surface *N*,*N*-chelated sites to form MOF-253 supported $[Ru(bpy)_2(X_2bpy)^{2+}]$, which is expected to show absorption in visible-light region (Figure 17).

The photocatalytic activity of the $[Ru(bpy)_2(X_2bpy)^{2+}]$-sensitized MOF-253-$Ru(CO)_2Cl_2$ was found to increase significantly as compared with the MOF-253 lacking the Ru photosensitizer unit. The amount of $HCOO^-$, CO, and H_2 produced in 8 h over sensitized MOF-253-$Ru(CO)_2Cl_2$ (with a molar ratio of the $Ru(bpy)_2Cl_2$/Ru-complex of 1:2) was determined to be 4.84 μmol, 1.85 μmol, and 0.72 μmol, which is much larger than those produced over the parent MOF-253-$Ru(CO)_2Cl_2$ under similar conditions. Furthermore, it was also found that the photocatalytic performance of the sensitized MOF-253-$Ru(CO)_2Cl_2$ is significantly influenced by the amount of immobilized $Ru(bpy)_2Cl_2$. The optimum activity achieved for the sensitized MOF-253-$Ru(CO)_2Cl_2$ was with a $Ru(bpy)_2Cl_2$/$Ru(CO)_2Cl_2$ molar ratio of 1:1, resulting in the formation of $HCOO^-$, CO, and H_2 with 8.23 μmol, 2.73 μmol and 1.91 μmol after 8 h. Although the amount of CO produced did not change much compared to the parent system without the sensitizer, the formation of $HCOO^-$ over the sensitized system was about 12 times that

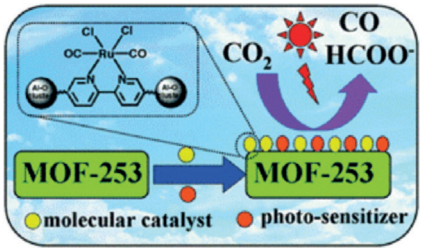

Figure 17. Schematic illustration of $[Ru(bpy)_2(X_2bpy)^{2+}]$ photosensitization of a modified MOF-253 containing $Ru(CO)_2Cl_2$ units as linkers that act as co-catalysts in CO_2 reduction to $HCOO^-$ (reproduced with permission from Ref. [102]).

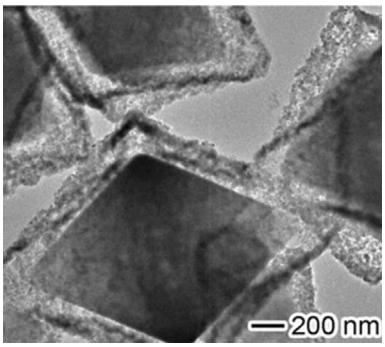

Figure 18. TEM image $Cu_3(BTC)_2@TiO_2$ core–shell structures showing the regular geometry of large $Cu_3(BTC)_2$ crystal surrounded by much smaller TiO_2 NPs (reproduced with permission from Ref. [104]).

over the system without the sensitizer (0.67 μmol), which corresponds to a TON of 35.8 for $HCOO^-$ formation.

Recently, UiO-67 was subjected to post-synthetic modification to replace bdc with a rhodium complex containing bpy units, namely, $Cp^*Rh(bpydc)Cl_2$ to achieve a rhodium-functionalized UiO-67 ($Cp^*Rh@UiO-67$).[103] The photocatalytic activity of the new catalyst was investigated in CO_2 reduction in CH_3CN and TEOA medium. The photocatalytic reduction of CO_2 using 10%-$Cp^*Rh@UiO-67$ (10% molar incorporation of Cp^*Rh approximately corresponding to 0.09 μmol Rh) resulted in a TON value of 47 towards the formation of $HCOO^-$ after 10 h, which is comparable with the free $Cp^*Rh(bpydc)Cl_2$ complex (0.08 μmol of Rh) to the TON of 42.[103] The temporal evolution of $HCOO^-$ upon irradiation in the presence of 10%-$Cp^*Rh@UiO-67$ and $Cp^*Rh(bpydc)Cl_2$ indicates comparable rates with comparable TOFs for $HCOO^-$ production of 7.5 and 10 h^{-1} for 10%-$Cp^*Rh@UiO-67$ and $Cp^*Rh(bpydc)Cl_2$, respectively. The 10%-$Cp^*Rh@UiO-67$ catalyst could be recycled up to six times, retaining the activity of the homogeneous system but displaying slightly higher rate for $HCOO^-$ and recyclability. Photocatalysts with higher Rh loadings show worse performance.

$Cu_3(BTC)_2@TiO_2$ core–shell structures have been prepared and their photocatalytic performance in gaseous CO_2 reduction have been examined.[104] The rationale behind the use of $Cu_3(BTC)_2@TiO_2$ is to combine the established photocatalytic activity for conversion of CO_2 into CH_4 with the aid of H_2O exhibited by TiO_2[131] with the excellent CO_2 storage capability of $Cu_3(BTC)_2$.[132] Therefore, the designed hybrid material possesses an optimal structure in which the semiconductor TiO_2 present as shells (210 nm thick, formed from small 10–20 nm NPs) can generate charge carriers while gaseous molecules can be captured at the cores. SEM analysis showed the core–shell structures inherit the octahedral morphology from the $Cu_3(BTC)_2$ cores and have a relatively rough surface (Figure 18). ICP-MS analysis showed the ratio of TiO_2 to $Cu_3(BTC)_2$ is approximately 0.5. The parent $Cu_3(BTC)_2$ and $Cu_3(BTC)_2@TiO_2$ core–shell structures exhibit CO_2 uptakes by weight of 80.75 and 49.17 $cm^3 g^{-1}$, respectively.

Bare TiO_2 gave 0.52 and 2.29 $\mu mol\, g_{TiO2}^{-1}\, h^{-1}$ of CH_4 and H_2, respectively, after 4 h under UV irradiation. On the other hand, $Cu_3(BTC)_2@TiO_2$ gave exclusively CH_4 (2.64 $\mu mol\, g_{TiO2}^{-1}\, h^{-1}$) under identical experimental conditions. These activity data demonstrate the superior performance of $Cu_3(BTC)_2@TiO_2$ in the selective reduction of CO_2 with an enhancement of the CH_4 yield with respect to that of TiO_2 by over five times and a complete selectivity to CH_4 without simultaneous generation of unwanted H_2. Although both TiO_2 and $Cu_3(BTC)_2$ can absorb UV light, $Cu_3(BTC)_2$ does not possess photocatalytic activity owing to its lack of semiconducting properties. In addition to the advantage in efficient CO_2 photoreduction, the designed heterostructures exhibit excellent photocatalytic stability in a recycling tests without showing any decrease in CH_4 yield in the 1st, 2nd, and 3rd runs, with strong resistance to morphology and composition changes. Further, it was demonstrated by ultrafast spectroscopy that the photogenerated electrons are effectively transferred from the semiconductor to the MOF, facilitating charge separation in the semiconductor and supplying electrons to CO_2 adsorbed on the MOF. It could have been, however, interesting to check the reverse situation in which TiO_2 is at the core of the composite and $Cu_3(BTC)_2$ at the shell. In this way, to reach photosensitized electrons at the semiconductor core, CO_2 adsorption on the MOF would be a prerequisite.

The combination of CdS and Co-ZIF-9 as photocatalyst and co-catalyst, respectively, can be used for the conversion of CO_2 into CO with visible light in the presence of bpy and TEOA under mild reaction conditions (Figure 19).[105] This photocatalytic system leads to the generation of CO (50.4 $\mu mol\, h^{-1}$) and H_2 (11.1 $\mu mol\, h^{-1}$) under visible-light irradiation.[105] As a control to establish the influence of the Co-ZIF-9 structure, the physical mixture of $Co(NO_3)_2{\cdot}6H_2O$ and benzimidazolate with CdS gave CO (40.3 $\mu mol\, h^{-1}$) and H_2 (7.5 $\mu mol\, h^{-1}$) under identical conditions. These results demonstrate some superiority of structured Co-ZIF-9 compared with its precursors in the reduction of CO_2 to CO. It was proposed that the Co-ZIF-9 co-catalyst enhances the photocatalytic conversion of CO_2 into CO with CdS by acting both as a CO_2 adsorber/activator and as a redox co-catalyst of the photoinduced charge separation. Besides CO, there were no other detectable products, such as HCOOH, CH_3OH or C–C coupling products. The accumulated TON with respect to Co-ZIF-9 for the photocatalytic CO_2 reduction was greater than 30. Adding a small amount (0.2 mg) of Co-ZIF-9 to the CdS photocatalytic system enhanced the catalytic performance in

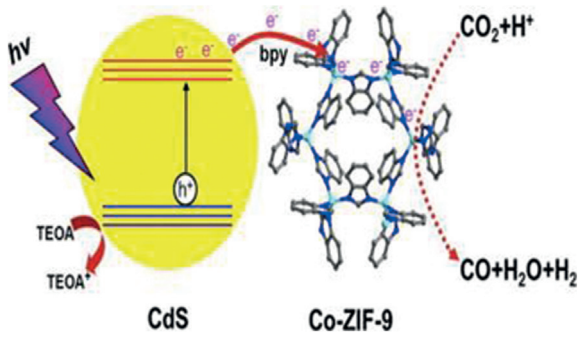

Figure 19. Schematic illustration of the photocatalytic system comprising CdS as a semiconductor and Co-ZIF-9 as a co-catalyst (reproduced with permission from Ref. [105]).

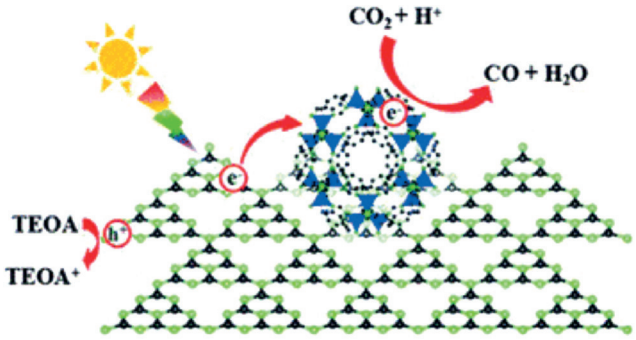

Figure 20. Schematic illustration of the Co-ZIF-9 supported on metal-free g-C_3N_4 semiconductor. Note that g-C_3N_4 is shown as single layers having triangular melon units sharing corners (reproduced with permission from Ref. [106]).

CO evolution about 45-times compared to the co-catalyst-free experiment. This comparison shows the promotional ability of the Co-ZIF-9 for CO_2 conversion by CdS photocatalysis. A maximum yield of CO (50.4 μmol) was achieved when 1 mg Co-ZIF-9 was added to the system. The production of H_2 increased gradually with the increasing amount of Co-ZIF-9 and was accompanied by a simultaneous decrease in the evolution of CO, which shows that the pathways for CO and H_2 formation are competing. It was also observed that the total production of CO and H_2 increased substantially as the reaction temperature increased from 10 to 40 °C, reaching a maximum value of 68.2 μmol at 40 °C. It would have been useful to check temperatures above 40 °C to determine if further productivity increase can be achieved for even higher temperatures. This influence of the reaction temperature suggests activation energy is required in the rate-determining step of the photocatalytic process that can be accelerated thermally. Furthermore, it was also observed that the product selectivity is greatly influenced by the H_2O content. On the other hand, when the reaction was performed in H_2O, the photocatalytic system was almost inactive to convert CO_2 into CO and only H_2 evolution was observed, a fact that can be attributed to the low solubility of CO_2 in H_2O at neutral or acid pH values.

A noble-metal-free system has been developed for the photochemical reduction of CO_2 under visible-light conditions by integrating graphitic carbon nitride (g-C_3N_4) with a cobalt-containing zeolitic imidazolate framework (Co-ZIF-9) (Figure 20).[106] The idea behind this hybrid catalyst is that g-C_3N_4 acts as a metal-free semiconductor photocatalyst, while Co-ZIF-9 is facilitating the capture/concentration of CO_2 and promotes light-induced charge separation. Under the optimized reaction conditions, the physical mixture of g-C_3N_4 and Co-ZIF-9 gave 20.8 μmol of CO and 3.3 μmol H_2 after 2 h irradiation in TEOA medium. The two materials cooperate efficiently to catalyze CO_2 into CO conversion upon visible-light illumination under mild reaction conditions. Even without noble metals, the system still exhibited an apparent quantum yield of 0.9 %. Furthermore, the system showed high photocatalytic stability, without noticeable alterations in the chemical and crystal structures of g-C_3N_4 and Co-ZIF-9 after the reaction and being reused seven times with no noticeable change in its activity.

Zn_2GeO_4/ZIF-8 hybrid nanorods were synthesized by growing ZIF-8 NPs on Zn_2GeO_4 nanorods and their photocatalytic activity was tested in the reduction of CO_2 to CH_3OH (Figure 21).[107] The Zn_2GeO_4 nanorods gave

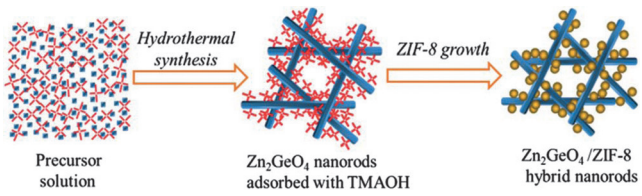

Figure 21. Illustration summarizing the preparation procedure for Zn_2GeO_4/ZIF-8 (reproduced with permission from Ref. [107]).

a CH_3OH yield of 1.43 μmol g^{-1} under light (500 W xenon arc) illumination for 10 h. In contrast, Zn_2GeO_4/ZIF-8 gave a CH_3OH yield of 2.44 μmol g^{-1}, corresponding to a CH_3OH formation rate of approximately 0.22 μmol $g^{-1}h^{-1}$. The use of Zn_2GeO_4/ZIF-8 as a photocatalyst showed a 62 % enhancement in CH_3OH yield when compared with the Zn_2GeO_4 after 10 h. The higher photocatalytic activity of the Zn_2GeO_4/ZIF-8 in the reduction of CO_2 relative to that of the Zn_2GeO_4 sample is attributed to the positive influence of ZIF-8. It is proposed that this synergism arises from the fact that ZIF-8 can effectively adsorb dissolved CO_2 in H_2O solution, and also, the light absorption is more intense for Zn_2GeO_4/ZIF-8 compared to Zn_2GeO_4 as evidenced by comparison of their UV/Vis spectra. Interestingly, the rate of CH_3OH generation was further improved by loading 1 wt % Pt over the Zn_2GeO_4/ZIF-8 nanorods to achieve CH_3OH yield around 3 μmol $g^{-1}h^{-1}$. Also, XRD patterns of the Zn_2GeO_4/ZIF-8 nanorods remained unchanged before and after the photocatalytic reaction, thus, indicating the stability of this hybrid photocatalyst under the reaction conditions. However, there were no data regarding the reusability which should provide additional crucial information on the stability of photocatalytic centers.

10. Photooxidation

Oxidation of alcohols to the corresponding aldehydes is one of the most important reactions in organic synthesis[133] because aldehydes and ketones are the starting materials for many synthesis, particularly in fine chemistry for the production of fragrances and flavors.[134] Table 3 summarizes those reports describing the use of MOFs as photocatalysts to promote photocatalytic oxidations, either in the absence or in the presence of an additional semiconductor.

Amine-functionalized UiO-66 (NH_2-UiO-66) has been reported as a visible-light photocatalyst for the selective aerobic oxygenation of various organic compounds including alcohols, olefins, and cycloalkanes, with high efficiency and high selectivity (Scheme 13).[135] As commented earlier, NH_2-UiO-66 and UiO-66 are isostructural and the presence of the -NH_2 group in the bdc linker introduces a new absorption band at 450 nm in the diffuse reflectance UV/Vis spectrum of NH_2-UiO-66. While none of the reactions occurred in the dark, visible-light irradiation of NH_2-UiO-66 increased the conversion of the studied alkenes monotonously with irradiation time. Control experiments showed that UiO-66 and ZrO_2 are catalytically inactive for all the substrates studied under the same conditions, confirming the unique role of the -NH_2 groups. The experimental results indicate that the final product selectivity is dependent on the nature of the solvent employed and on the reacting substrates. For example, epoxides were obtained from β-methylstyrene, styrene, and 1,2-diphenylethylene with selectivity values ranging from 15 to 65%. In contrast, cyclooctene resulted in low conversion owing to its larger kinetic diameter compared to the pore size of NH_2-UiO-66 (5.1 Å), but gives 100% selectivity to cyclooctene epoxide as result of its favorable geometrical conformation. These results suggest that the selectivity to epoxide is closely related to the chemical stability of the intermediates formed during the photocatalytic process. An ^{18}O-isotope labelling experiment for the photocatalytic epoxidation of cyclooctene confirmed that oxygen in the product comes from molecular oxygen present in the gas phase, thus, convincingly confirming the occurrence of photocatalytic oxidation reactions. Furthermore, benzyl alcohol, cyclohexanol, 1-hexanol, and cyclohexane were tested to show the wide applicability of NH_2-UiO-66 as a photocatalyst promoting oxidation reactions. A complete selectivity was achieved for these four substrates, although, the rate of reaction mainly depends on the energy of α-C-H bonds, decreasing in the order of benzyl alcohol > cyclohexanol > 1-hexanol > cyclohexane. Also, ESR spectroscopy showed the formation of the superoxide radical anion ($O_2^{-\bullet}$). This species could be stabilized in the cavities of NH_2-UiO-66 through its interaction with the -NH_2 groups and/or organic solvents. The long lifetime of $O_2^{\bullet-}$ should be beneficial for the photocatalytic oxygenations of C–H and C=C bonds. Studies on catalyst stability and its reusability should confirm that the reactive oxygen species generated in the process do not decompose or self degrade NH_2-UiO-66 during operation of the photocatalytic oxidation.

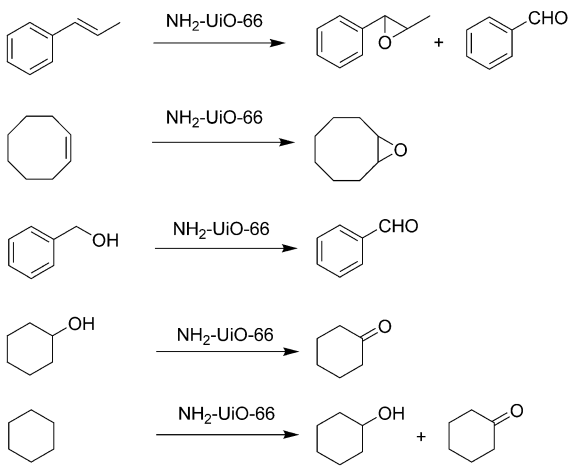

Scheme 13. Photooxidation of various substrates catalyzed by NH_2-UiO-66.

CdS nanorods have been deposited on the surface of NH_2-UiO-66 via a facile room-temperature photodeposition to obtain CdS-NH_2-UiO-66 nanocomposites that were used as photocatalysts for the selective oxidation of various alcohols by molecular oxygen (Scheme 14).[136] A series of CdS-NH_2-UiO-66 derivatives was prepared employing different CdS photodeposition times. ICP analysis shows that the percentage of Cd in CdS-U6 (CdS-NH_2-UiO-66 with 6 h irradiation time) is 30.02%. TEM images revealed that NH_2-UiO-66

Table 3: Summary of photooxidation reactions catalyzed using MOFs-based photocatalysts.

Catalyst	Photolysis source	Photoactivity	Stability evidence	Ref.
NH_2-UiO-66	300 W Xe lamp	1.234 h^{-1} (TOF)[a]	–	[135]
CdS-NH_2-UiO-66	300 W Xe arc lamp	31% conversion[b]	XRD, XPS, reuse	[136]
NH_2-UiO-66-F	26 W helical light bulb	53.9% conversion[b]	–	[137]
multicore Au@ZIF-8	500 W Xe lamp	51.6% conversion[b]	–	[138]
Au/MIL-125(Ti)	300 W Xe arc lamp (λ = 320–780 nm)	36% conversion[b]	–	[94]
NH_2-MIL-125(Ti)	300 W Xe lamp	73% conversion[c]	XRD, reuse	[139]
MR-MIL-125(Ti)[d]	150 W Xe lamp	86.7 nmol g^{-1} min^{-1}[b]	reuse	[140]
TiO_2@HKUST-1[e]	sunlight	89% conversion[b]	IR, XRD, reuse,	[141]
UiO-67-$[Ru(bpy)_3]_{0.1}$	photochemical reactor (λ = 365 nm)	81% yield	reuse, ICP-OES	[142]

[a] Data corresponds to the oxidation of β-methylstyrene. [b] Oxidation of benzyl alcohol. [c] Oxidation of benzyl amine. [d] MR: methyl red. [e] HKUST-1: Hong Kong University of Science and Technology.

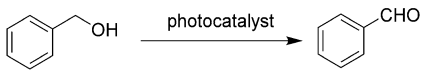

Scheme 14. Photocatalytic oxidation of benzyl alcohol.

serves as support and its characteristic structure is retained. In addition, HRTEM images of CdS-U6 showed the lattice fringes corresponding to CdS, suggesting the well-defined crystal structure of CdS (Figure 22). UV/Vis absorption

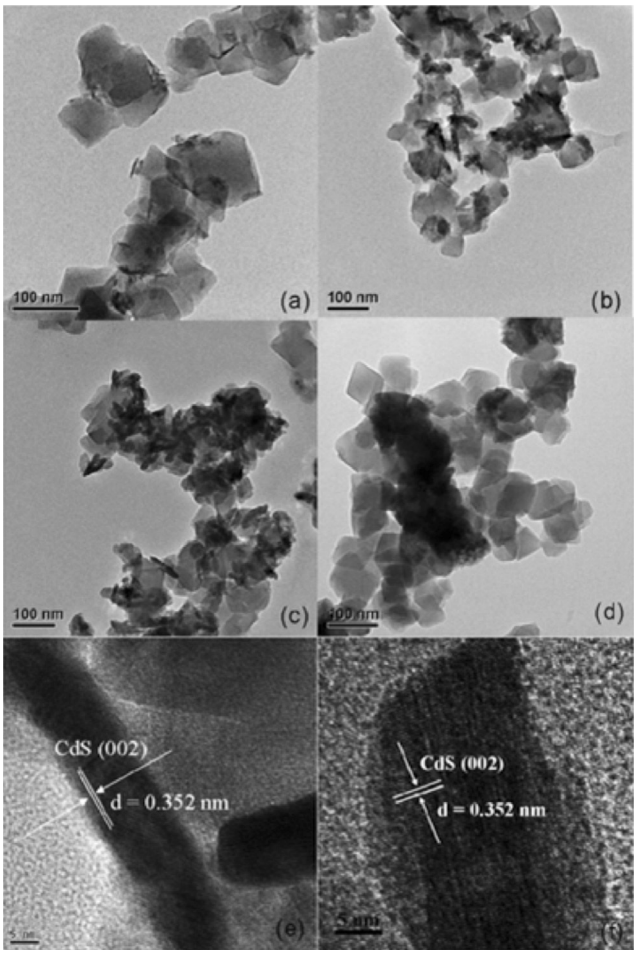

Figure 22. TEM images for the CdS-NH_2-UiO-66 nanocomposites prepared by photodeposition for 2, 4, 6, and 8 h (a–d) and HRTEM images of CdS-U6 (e,f; reproduced with permission from Ref. [136]).

spectra of CdS-NH_2-UiO-66 nanocomposites clearly indicated that the absorption edge red-shifts and absorption intensity increases as a result of the increase in irradiation time, the onset varying gradually from 450 nm to nearly 530 nm, owing to the increase in CdS nanocrystal size with prolonged irradiation time.

The photocatalytic activity of the as-prepared CdS-NH_2-UiO-66 nanocomposites was examined for the selective oxidation of benzyl alcohol to benzaldehyde under visible-light irradiation. The optimal photocatalytic activity was achieved with CdS-U6 exhibiting 31 % conversion of benzyl alcohol with 100 % selectivity of benzaldehyde after 4 h. On the other hand, CdS-U8 showed around 13 % conversion of benzyl alcohol with less than 50 % selectivity of benzaldehyde. These photocatalytic data clearly show that increasing CdS photodeposition time beyond a certain time leads to a deterioration of the photocatalytic activity, mainly because the CdS nanocrystals become bigger and aggregate on the MOF surface, resulting in a reduced surface area of the sample. Under identical conditions, NH_2-UiO-66, CdS, and the physical mixture of NH_2-UiO-66 and CdS resulted in 20, 9, and 17 % conversions of benzyl alcohol, respectively, with the selectivity of benzaldehyde less than 60 %. These results clearly establish the superior performance of CdS-U6 in terms of conversion and product selectivity. Furthermore, the photocatalytic activity of CdS-U6 was tested for a series of alcohols under identical conditions, reaching moderate conversions and high selectivities. CdS-U6 was reused five times for the selective oxidation of benzyl alcohol with no obvious decrease in activity. In contrast, the photocatalytic activity of commercial CdS decreased notably in the recycling experiments. These results show the superior performance of CdS-U6 and higher stability than bare CdS owing to interaction with NH_2-UiO-66 surface. The powder XRD and XPS measurements of CdS-U6 before and after use as a photocatalyst showed no significant changes.

A series of mixed-linker zirconium-based metal–organic frameworks (Zr-MOFs) containing 2-amino-1,4-benzenedicarboxylate as the primary linker and 2-X-1,4-bezenedicarboxylate (X = H, F, Cl and Br) as a secondary linker has been synthesized to evaluate their photoactivity in the oxidation of benzyl alcohol under visible-light irradiation. Powder XRD patterns showed that the Zr-MOFs synthesized with the mixed linkers are crystalline and isoreticular to the parent UiO-66. The conversion of benzyl alcohol was 18.4 % using NH_2-UiO-66 as catalyst after 24 h. When the concentration of 2-atp linkers was reduced by half as in NH_2-UiO-66 which contains 45 % 2-atp, the remaining 55 % of the linker is bdc, the benzyl alcohol conversion decreased to 11.7 %. Among the various catalysts examined, NH_2-UiO-66-F, NH_2-UiO-66-Cl, and NH_2-UiO-66-Br exhibited 53.9, 38.2, and 43.4 % conversions of benzyl alcohol under identical conditions. These experiments clearly establish that replacement of bdc linkers by halogenated analogues (X-bdc, X = F, Cl, Br) leads to a four- to five-fold enhancement of the photocatalytic activity for the benzyl alcohol oxidation in comparison to NH_2-UiO-66. This could be due to the stabilization of the superoxide radical anion on the Zr^{3+} by the halogenated linkers, decreasing the recombination rate of the photogenerated electrons and holes. Other possible reasons for this enhancement in the catalytic activity could also be related to the preferential interaction of the halogen groups with benzyl alcohol molecules driving the equilibrium of the reaction to benzaldehyde.

A series of samples of Au encapsulated in ZIF-8 (Au@ZIF-8) containing spherical or rod-like shaped AuNPs embedded in single- or multi-core–shell nanocrystals of ZIF-8 (Figure 23) has been prepared and their photocatalytic activity studied for the oxidation of benzyl alcohol (Scheme 14).[138] TEM images revealed that the Au@ZIF-8

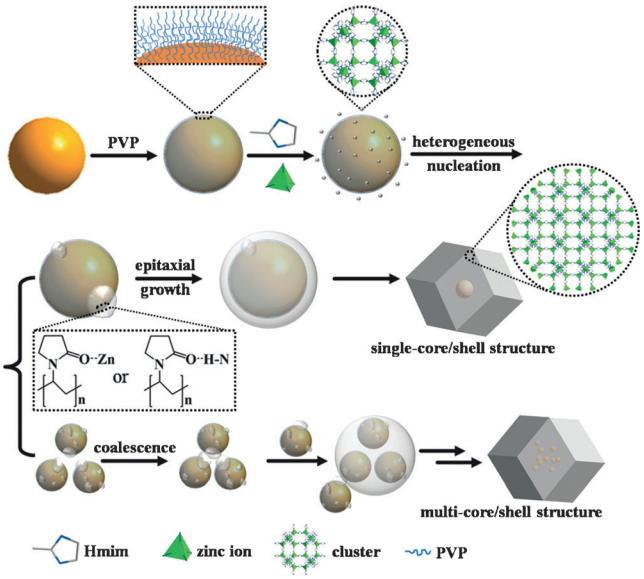

Figure 23. Synthetic procedure used for the preparation of single- or multi-core polyvinylpyrrolidone-stabilized Au NPs embedded inside the crystal structure of ZIF-8 (reproduced with permission from Ref. [138]).

core–shell sample consists in a distribution of single (48%), double-, and triple-core (45%), as well as Au NPs-free ZIF-8 nanocrystals (7%). The size distribution of the MOF component in the Au@ZIF-8 composite ranges from 135 to 200 nm, and there was no apparent change in the diameter of the Au NPs during the preparation of the composite.

The powder XRD pattern of Au@ZIF-8 did not show any difference to that of ZIF-8, while TEM images clearly showed that the ZIF-8 shell adopts the thermodynamically favorable rhombic dodecahedron form.[143] Photocatalytic oxidation of benzyl alcohol was performed in CH_3CN in the presence of single- or multi-core Au@ZIF-8 photocatalysts with a Xe lamp fitted with a cut-off filter ($\lambda > 400$ nm). Single-core and multi-core Au@ZIF-8 exhibited 25.8 and 51.6% conversions, respectively, after 24 h irradiation, with a selectivity to benzaldehyde of over 99% for both cases. This difference in conversion indicates the benefits of combining plasmonic light absorption by Au NPs with multi-core ZIF-8 structures. In contrast, Au-SiO_2 resulted in 56.9% conversion under identical reaction conditions. This difference in conversion can be attributed to the ZIF-8 restricting benzyl alcohol diffusion in the pore cavities making it harder for it to reach the Au NPs, thus resulting in the decrease of photocatalytic activity.

The photocatalytic activity of MIL-125(Ti) and M/MIL-125(Ti) (M = Au, Pd, and Pt NPs) composites was studied in the oxidation of benzyl alcohol to benzaldehyde.[94] TEM images revealed that the small Au, Pd, and Pt NPs are homogeneously distributed on the MIL-125(Ti) with the average diameters of Au, Pd, and Pt being 6, 3, and 3 nm, respectively. MIL-125(Ti) showed a conversion of 18.9% with >99% benzaldehyde selectivity. Under identical conditions, Au/MIL-125(Ti), Pd/MIL-125(Ti), and Pt/MIL-125(Ti) catalysts exhibited 36, 32.7, and 26.4% conversions, respectively with >99% selectivity of benzaldehyde. These experiments clearly show the effect of metal NPs in promoting the reaction by enhancing the conversion of benzyl alcohol.

Recently, NH_2-MIL-125(Ti) has been reported to effect the photocatalytic aerobic oxidation of amines to imines under visible-light irradiation.[139] Under optimized reaction conditions, NH_2-MIL-125(Ti) gave 73% conversion of benzyl amine with 86% selectivity to *N*-benzylidene benzyl amine (Scheme 15). Furthermore, primary and secondary amines

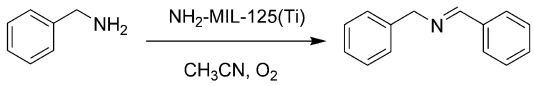

Scheme 15. Photocatalytic oxidation of benzyl amine by NH_2-MIL-125-(Ti) under aerobic conditions.

were also transformed into the corresponding imines with moderate conversions (53–73%) and selectivities (70–94%) using O_2 in the presence of NH_2-MIL-125(Ti) under visible-light irradiation. In addition, benzaldoxime and benzaldehyde were produced as byproducts in these reactions. Control experiments showed that the reaction is heterogeneous. Furthermore, NH_2-MIL-125(Ti) after the photocatalytic reaction showed similar XRD patterns as that of the fresh catalyst. The catalyst was reused for three runs showing no obvious decrease in activity.

NH_2-MIL-125(Ti) has been post-synthetically functionalized with dye-like molecular fragments to obtain methyl red-MIL-125(Ti) (MR-MIL-125(Ti); Figure 24).[140] The resulting MR-MIL-125(Ti) was tested as photocatalyst for the selective oxidation of benzaldehyde under visible-light irradiation.[140] Quantitative analysis indicated that 26 to 30% of the linkers are functionalized. This relatively low degree of functionalization is not unexpected in view of the bulkiness of the MR moiety. NH_2-MIL-125(Ti) exhibited two absorption bands at 325 and 465 nm attributed to the electronic transition from 2-atp^{2-}Ti^{4+} to 2atp^{-}Ti^{3+} subunits of the framework,[96,144] whereas MR-MIL-125(Ti) showed a clear red shift with the

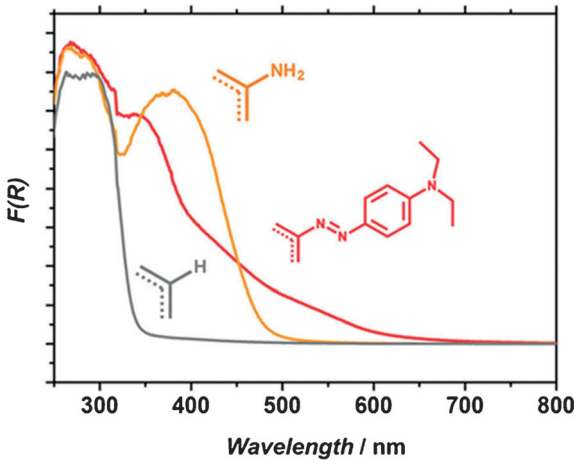

Figure 24. Diffuse reflectance UV/Vis spectra of MIL-125(Ti) (gray), NH_2-MIL-125(Ti) (orange) and the methyl red analogue (red; reproduced with permission from Ref. [140]).

absorption edge reaching almost 700 nm (Figure 24). This significant visible-light absorption enhancement can be associated to the presence of the MR moiety after the modification. The long-wavelength absorption maxima of the MOF suggests that most of the modified linkers have the aza group in the *trans* form, since the *cis*- and *trans* isomers of the analogous MR molecule embedded in rigid polymers absorb at < 400 and 565 nm, respectively.[145]

The photocatalytic activity of MR-MIL-125(Ti) was assessed in the selective oxidation of benzyl alcohol to benzaldehyde in CH_3CN with light of wavelength longer than 400 nm. Both NH_2-MIL-125 and MR-MIL-125 were found to be active under visible-light illumination with the benzaldehyde formation reaction rates of 77.6 and 86.7 nmol g^{-1} min^{-1}, respectively. MR-MIL-125(Ti) was recycled two times without loss of activity. Note that bulk TiO_2 was found to be deactivated in a similar photo-oxidation reaction owing to irreversible product adsorption.[146] The enhanced photocatalytic activity of MR-MIL-125(Ti) compared to the parent framework was attributed to the higher light absorption resulting from the extended conjugation of the aromatic system as a consequence of ligand modification. However, the absolute enhancement of the photocatalytic activity is lower than it could have been expected suggesting that the system can possible be subjected to further optimization.

Mesoporous HKUST-1 decorated with amorphous TiO_2 has been reported as a photocatalyst for the selective aerobic oxidation of alcohols under sunlight irradiation (Scheme 16).[141] Different amounts of P123 were used to

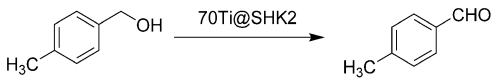

Scheme 16. Aerobic oxidation of 4-methylbenzyl alcohol catalyzed by TiO_2-modified SHK.

determine the optimum surfactant in the surfactant-assisted synthesis of HKUST-1 (SHK). A control HKUST-1 sample was also synthesized in the absence of structure-directing agent P123. The powder XRD pattern of all the samples prepared with and without P123 coincide with that reported for HKUST-1.[147] TEM images suggested that SHK consists of ordered mesoporous domains of the parent MOF having microporous structure (Figure 25). The surface of SHK was decorated with amorphous titania through a layer-by-layer coating.[148] Powder XRD, IR, and SEM analysis supported that the crystalline nature or structure of the parent MOF remained intact after titania embedding.

The photocatalytic performance of these nanocomposite materials was evaluated for the aerobic oxidation of 4-methylbenzyl alcohol as a model substrate in CH_3CN under sunlight irradiation. The photocatalysts were able to achieve up to 89% conversion of 4-methylbenzaldehyde with high selectivity ($> 93\%$).[141] No photocatalytic activity was observed in the presence of bare HKUST-1 after 15 h of irradiation. The photocatalytic reactivity of SHK arises to a large extent from the uniform mesostructure of TiO_2-

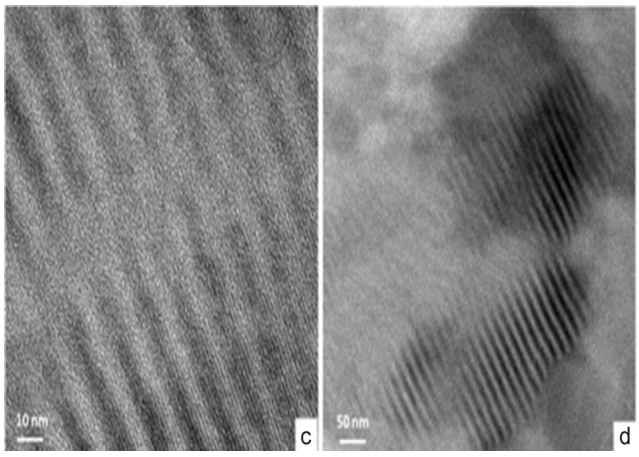

Figure 25. Two representative TEM images corresponding to TiO_2 deposited on SHK (reproduced with permission from Ref. [141]).

modified SHK and assumes that the reaction takes place inside the pores of the mesoporous structure. Furthermore, TiO_2-modified SHK was an active photocatalyst to transform primary and secondary benzylic alcohols into their corresponding carbonyl compounds with high selectivities (93–99%) and moderate to high conversions (32–100%).[141] The recycled photocatalyst still retains a large percentage of the initial activity of the fresh material upon sunlight irradiation. The decrease in photocatalytic activity was attributed to structural changes upon catalyst use. Although Ti@SHK2 represents a step forward in the search of a multicomponent photocatalyst that combines the advantage of porosity, large surface area, and activity of MOFs with that of conventional semiconductors, it is evident that there are still certain limitations that have to be overcome to reach higher efficiency. In particular, it is well known that amorphous TiO_2 has low activity compared to highly crystalline anatase phase materials and thus it would be worth investigating composites with high TiO_2 crystallinity.

Recently, a photocatalytically active $[Ru(bpy)_2(dcbpy)]^{2+}$ complex (dcbpy: 5,5′-dicarboxy-2,2′-bipyridine) was incorporated into a UiO-67 MOF via postsynthetic modification to obtain UiO-67-$[Ru(bpy)_3]_{0.1}$ with approximately 10% Ru loading and its photocatalytic activity was examined for the aerobic oxidation of arylboronic acids to the corresponding phenols under near-UV and visible-light irradiation.[142] The optimized reaction conditions using UiO-67-$[Ru(bpy)_3]_{0.1}$ as a photocatalyst in MeOH gave an 81% yield of phenol using a photochemical reactor ($\lambda = 365$ nm) after 24 h. However, this yield was slightly lower than a homogeneous catalyst, namely $(Ru(bpy)_3Cl_2$ which shows 95% yield. In contrast, pristine UiO-67-$bpy_{0.25}$ gave 22% conversion under UV irradiation after 24 h. Also, oxygen was found to be the real oxidant as the reaction in inert atmosphere results in no product. The catalyst was reused four times, exhibiting in each run high yields, but, however, with slightly decreasing activity. Leaching experiments revealed that UiO-67-$[Ru(bpy)_3]_{0.1}$ is acting as a heterogeneous catalyst. ^{1}H NMR spectrum showed that there is low leaching of the Ru complex from the MOF after one catalytic run. Furthermore, ICP-OES analysis

showed an atomic ratio of 1:0.106 (Zr/Ru) for the five-times reused UiO-67-$[Ru(bpy)_3]_{0.1}$, which is about 10% lower than for the fresh catalyst which has an atomic ratio of 1:0.118 (Zr/Ru).

11. Photoreduction

Photocatalysis leading to charge separation can serve to promote oxidations (by the reaction with positive holes) and reduction (with conduction-band electrons). In fact, both processes should take place at the same rate, but depending upon the substrate only one of the two half-reactions can occur. For the present Review, reductions are the most wanted process as solar fuels production is generally a reduction process. As commented in the previous Sections, generation of H_2 from H_2O and CH_4, CO, and HCO_2H from CO_2 are reduction reactions. Below we will present other different photocatalytic reductions mainly of aromatic nitro groups.

Pt/NH_2-Ti-MOF was found to act as a photocatalyst for the reduction of nitrobenzene under visible-light irradiation (500 W Xe lamp) using TEOA as a sacrificial electron donor, leading to aniline as the final product (Scheme 17).[93] Nitrobenzene was found to be a reaction intermediate. Under the optimized reaction conditions, Pt(1.5)/NH_2-Ti-MOF (3.3 μmol h^{-1}) exhibited higher photocatalytic activity than NH_2-Ti-MOF (2.3 μmol h^{-1}) indicating that deposited Pt also acts as a co-catalyst in this system. It was observed that selectivities of the reaction are almost the same regardless of the presence of Pt species. On the other hand, no reaction occurred in the absence of visible light. The reaction failed with Pt(1.5)/Ti-MOF or with a physical mixture of Pt(1.5)/Ti-MOF and 2-atp as a photocatalyst. These control experiments clearly indicate that the crystal structure of NH_2-Ti-MOF comprising coordination networks of Ti-oxo clusters and 2-atp units are responsible for the photocatalytic reaction. Recycling tests indicated no significant loss of photocatalytic activity even after four cycles. Furthermore, powder XRD and FT-IR measurements showed no significant changes in the fresh and repeatedly used Pt(1.5)/NH_2-Ti-MOF photocatalyst, indicating a high stability under the reaction conditions.

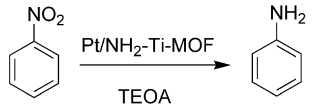

Scheme 17. Photoreduction of nitrobenzene catalyzed by Pt(1.5)/NH_2-Ti-MOF.

12. Summary and Concluding Remarks

In the previous Sections, it has been shown that although MOFs are relatively new materials, they have been increasingly attracting interest as photocatalysts and now this field constitutes a current hot topic in photocatalysis. The main reason for this interest is the functionality introduced by the organic linkers and the possibility to adapt the MOF for this specific application, particularly in contrast to TiO_2 and inorganic semiconductors. As we have shown, there is still considerable room for expanding the use of MOFs as photocatalysts for the synthesis of fine chemicals, mainly for oxidations and reductions, taking advantage of the charge separation that appears as a quite general phenomenon in the photophysics of MOFs. The advantages that MOFs offer for the design of new photocatalysts have been presented and this strategy should be intensely developed in the near future. With respect to photocatalytic H_2 generation and CO_2 reduction, it is clear that there are many possible strategies to increase the efficiency of MOFs, one of the main problems is to establish valid comparisons of the photocatalytic activity of various materials. In any case, from perusal of Table 1 it can be concluded that the highest H_2 production reported to date is about 2–3.5 mmol, achieved using modified UiO-66 or $[Ln_2Cu_5(OH)_2(pydc)_6(H_2O)_8]\cdot I_8$. In the case of CO_2 photoreduction, most of the studies have been carried out in water or acetonitrile, leading to the formation of $HCOO^-$ and, the most active photocatalysts are again modified UiO-66, but also MIL-101(Fe) with production values from 13 to about 175 μmol. It should be noted that almost all the examples reported so far make use of sacrificial agents to demonstrate the concept of their photocatalytic activity. However, for practical application in H_2 generation or CO_2 reduction, the use of sacrificial agents is not possible and processes such as overall H_2O splitting or photocatalytic CO_2 reduction by H_2O have to be used, particularly using natural sunlight. In overall H_2O splitting, H_2 and O_2 should be generated in the corresponding stoichiometric amount by solar light in the absence of amines, alcohols, or any other additive. At the moment there are limited examples showing that MOFs are able to promote photocatalytic overall H_2O splitting.

Similarly, CO_2 reduction either to CH_4 or CH_3OH, $HCOO^-$ or CO has to be performed using H_2O as the electron donor agent, as happens in natural photosynthesis, without using amines or sacrificial agents. This fundamental reaction has also not been reported so far using MOFs. It is clear that the target of this area should be the development of materials and processes that could be economically feasible for the production of solar fuels. Furthermore, MOFs as photocatalysts should also be tested for other photocatalytic reactions that could be of interest in an integrated solar refinery, particularly the photoassisted reduction of CO_2 by H_2 that should be produced electrochemically from electricity from renewable sources.

We are still very far from this long-term target that would require a jump in the photocatalytic activity of one or two orders of magnitude in the case of H_2 generation and four or more orders of magnitude in the case of CO_2 reduction. However, the current state-of-art has shown that MOFs are among the best positioned materials to perform this jump in catalytic activity.

Acknowledgements

Financial support by the Spanish Ministry of Economy and Competitiveness (CTQ-2015-69153-C2-1-R and Severo Ochoa) and Generalidad Valenciana (Prometeo 2013-014) is gratefully acknowledged. The research leading to these results has received partial funding from the European Community's Seventh Framework Programme (FP7/2007-2013) under grant agreement no. 228862. A.D.M. thanks University Grants Commission, New Delhi for the award of Assistant Professorship under its Faculty Recharge Programme. A.D.M. also thanks Department of Science and Technology, India, for the financial support through Fast Track project (SB/FT/CS-166/2013).

How to cite: *Angew. Chem. Int. Ed.* **2016**, *55*, 5414–5445
Angew. Chem. **2016**, *128*, 5504–5535

[1] N. J. Turro, V. Ramamurthy, J. C. Scaiano, *Principles of Molecular Photochemistry: An Introduction*, University Science Books, New York, **2010**.
[2] E.-Z. M. Ebeid, *Photophysical and Laser Based Techniques in Chemistry, Biology, and Medicine*, BookSurge Publishing, Charleston, **2006**.
[3] V. Ramamurthy, *Photochemistry in Confined Spaces*, VCH, New York, **1991**.
[4] L. J. Johnston, P. De Mayo, S. K. Wong, *J. Org. Chem.* **1984**, *49*, 20.
[5] P. de Mayo, K. Okada, M. Rafalska, A. C. Weedon, G. S. K. Wong, *J. Chem. Soc. Chem. Commun.* **1981**, 820.
[6] V. Ramamurthy, N. Turro, *J. Inclusion Phenom. Mol. Recognit. Chem.* **1995**, *21*, 239.
[7] J. C. Scaiano, H. García, *Acc. Chem. Res.* **1999**, *32*, 783.
[8] V. Ramamurthy, D. R. Corbin, N. J. Turro, Z. Zhang, M. A. Garcia Garibay, *J. Org. Chem.* **1991**, *56*, 255.
[9] A. Corma, H. Garcia, *Chem. Commun.* **2004**, 1443.
[10] V. Ramamurthy, D. F. Eaton, J. V. Caspar, *Acc. Chem. Res.* **1992**, *25*, 299.
[11] M. R. Hoffmann, S. T. Martin, W. Y. Choi, D. W. Bahnemann, *Chem. Rev.* **1995**, *95*, 69.
[12] A. L. Linsebigler, G. Q. Lu, J. T. Yates, *Chem. Rev.* **1995**, *95*, 735.
[13] M. A. Nasalevich, M. van der Veen, F. Kapteijn, J. Gascon, *CrystEngComm* **2014**, *16*, 4919.
[14] A. Hagfeldt, G. Boschloo, L. Sun, L. Kloo, H. Pettersson, *Chem. Rev.* **2010**, *110*, 6595.
[15] B. O'Regan, M. Gratzel, *Nature* **1991**, *353*, 737.
[16] M. Grätzel, *Inorg. Chem.* **2005**, *44*, 6841.
[17] A. Hagfeldt, M. Grätzel, *Acc. Chem. Res.* **2000**, *33*, 269.
[18] B. O'Regan, M. Grätzel, *Nature* **1991**, *353*, 737.
[19] N. Bao, L. Shen, T. Takata, K. Domen, *Chem. Mater.* **2008**, *20*, 110.
[20] H. Weller, *Angew. Chem. Int. Ed. Engl.* **1993**, *32*, 41; *Angew. Chem.* **1993**, *105*, 43.
[21] M. Anpo, M. Takeuchi, *J. Catal.* **2003**, *216*, 505.
[22] P. V. Kamat, *J. Phys. Chem. C* **2007**, *111*, 2834.
[23] S. C. Roy, O. K. Varghese, M. Paulose, C. A. Grimes, *ACS Nano* **2010**, *4*, 1259.
[24] G. Férey, *Chem. Soc. Rev.* **2008**, *37*, 191.
[25] S. Kitagawa, R. Kitaura, S. Noro, *Angew. Chem. Int. Ed.* **2004**, *43*, 2334; *Angew. Chem.* **2004**, *116*, 2388.
[26] O. M. Yaghi, M. O'Keeffe, N. W. Ockwig, H. K. Chae, M. Eddaoudi, J. Kim, *Nature* **2003**, *423*, 705.
[27] M. Eddaoudi, J. Kim, N. Rosi, D. Vodak, J. Wachter, M. O'Keeffe, O. M. Yaghi, *Science* **2002**, *295*, 469.
[28] J.-R. Li, R. J. Kuppler, H.-C. Zhou, *Chem. Soc. Rev.* **2009**, *38*, 1477.
[29] N. L. Rosi, J. Eckert, M. Eddaoudi, D. T. Vodak, J. Kim, M. O'Keeffe, O. M. Yaghi, *Science* **2003**, *300*, 1127.
[30] K. G. M. Laurier, F. Vermoortele, R. Ameloot, D. E. De Vos, J. Hofkens, M. B. J. Roeffaers, *J. Am. Chem. Soc.* **2013**, *135*, 14488–14491.
[31] A. Corma, H. Garcia, F. X. Llabres i Xamena, *Chem. Rev.* **2010**, *110*, 4606.
[32] Y. Cui, Y. Yue, G. Qian, B. Chen, *Chem. Rev.* **2012**, *112*, 1126.
[33] S. L. James, *Chem. Soc. Rev.* **2003**, *32*, 276.
[34] C. Janiak, *Dalton Trans.* **2003**, 2781.
[35] A. Dhakshinamoorthy, M. Alvaro, A. Corma, H. Garcia, *Dalton Trans.* **2011**, *40*, 6344.
[36] M. de Miguel, F. Ragon, T. Devic, C. Serre, P. Horcajada, H. Garcia, *ChemPhysChem* **2012**, *13*, 3651.
[37] K. G. M. Laurier, E. Fron, P. Atienzar, K. Kennes, H. Garcia, M. Van der Auweraer, D. E. De Vos, J. Hofkens, M. B. J. Roeffaers, *Phys. Chem. Chem. Phys.* **2014**, *16*, 5044.
[38] F. X. L. i. Xamena, A. Corma, H. Garcia, *J. Phys. Chem. C* **2007**, *111*, 80.
[39] T. Zhang, W. Lin, *Chem. Soc. Rev.* **2014**, *43*, 5982.
[40] C.-C. Wang, J.-R. Li, X.-L. Lv, Y.-Q. Zhang, G. Guo, *Energy Environ. Sci.* **2014**, *7*, 2831.
[41] K. Meyer, M. Ranocchiari, J. A. van Bokhoven, *Energy Environ. Sci.* **2015**, *8*, 1923.
[42] S. Wang, X. Wang, *Small* **2015**, *11*, 3097.
[43] T. Tachikawa, S. Tojo, M. Fujitsuka, T. Sekino, T. Majima, *J. Phys. Chem. B* **2006**, *110*, 14055.
[44] T. Loiseau, C. Serre, C. Huguenard, G. Fink, F. Taulelle, M. Henry, T. Bataille, G. Férey, *Chem. Eur. J.* **2004**, *10*, 1373.
[45] M. Dan-Hardi, C. Serre, T. Frot, L. Rozes, G. Maurin, C. Sanchez, G. Ferey, *J. Am. Chem. Soc.* **2009**, *131*, 10857.
[46] Q. Liu, Y.-N. Li, H.-H. Zhang, B. Chen, C.-H. Tung, L.-Z. Wu, *Chem. Eur. J.* **2012**, *18*, 620.
[47] Y. Yamakoshi, N. Umezawa, A. Ryu, K. Arakane, N. Miyata, Y. Goda, T. Masumizu, T. Nagano, *J. Am. Chem. Soc.* **2003**, *125*, 12803.
[48] H. G. Baldovi, M. Krueger, H. Reinsch, M. Alvaro, N. Stock, H. Garcia, *J. Mater. Chem.* **2015**, *25*, 3607.
[49] X.-L. Hu, C.-Y. Sun, C. Qin, X.-L. Wang, H.-N. Wang, E.-L. Zhou, W.-E. Li, Z.-M. Su, *Chem. Commun.* **2013**, *49*, 3564.
[50] R. Asahi, T. Morikawa, T. Ohwaki, K. Aoki, Y. Taga, *Science* **2001**, *293*, 269.
[51] C. Burda, Y. B. Lou, X. B. Chen, A. C. S. Samia, J. Stout, J. L. Gole, *Nano Lett.* **2003**, *3*, 1049.
[52] D. Panayotov, P. Kondratyuk, J. J. T. Yates, *Langmuir* **2004**, *20*, 3674.
[53] M. Jin, X. T. Zhang, A. V. Emeline, Z. Y. Liu, D. A. Tryk, T. Murakami, A. Fujishima, *Chem. Commun.* **2006**, 4483.
[54] S. Yanagida, A. Nakajima, T. Sasaki, Y. Kameshima, K. Okada, *Chem. Mater.* **2008**, *20*, 3757.
[55] Y. Hou, X. Y. Li, Q. D. Zhao, X. Quan, G. H. Chen, *Environ. Sci. Technol.* **2010**, *44*, 5098.
[56] P. D. Tran, L. H. Wong, J. Barber, J. S. C. Loo, *Energy Environ. Sci.* **2012**, *5*, 5902.
[57] H. Y. Yang, S. F. Yu, S. P. Lau, X. W. Zhang, D. D. Sun, G. Jun, *Small* **2009**, *5*, 2260.
[58] W. J. Youngblood, S.-H. A. Lee, K. Maeda, T. E. Mallouk, *Acc. Chem. Res.* **2009**, *42*, 1966.
[59] H. Hagiwara, T. Inoue, K. Kaneko, T. Ishihara, *Chem. Eur. J.* **2009**, *15*, 12862.
[60] J. Yano, V. Yachandra, *Chem. Rev.* **2014**, *114*, 4175.
[61] K. Watanabe, D. Menzel, N. Nilius, H.-J. Freund, *Chem. Rev.* **2006**, *106*, 4301.

[62] E. V. Chulkov, A. G. Borisov, J. P. Gauyacq, D. Sanchez-Portal, V. M. Silkin, V. P. Zhukov, P. M. Echenique, *Chem. Rev.* **2006**, *106*, 4160.
[63] M. E. Stewart, C. R. Anderton, L. B. Thompson, J. Maria, S. K. Gray, J. A. Rogers, R. G. Nuzzo, *Chem. Rev.* **2008**, *108*, 494.
[64] K. Kneipp, H. Kneipp, J. Kneipp, *Acc. Chem. Res.* **2006**, *39*, 443.
[65] W. A. Murray, W. L. Barnes, *Adv. Mater.* **2007**, *19*, 3771.
[66] P. K. Jain, X. H. Huang, I. H. El-Sayed, M. A. El-Sayed, *Acc. Chem. Res.* **2008**, *41*, 1578.
[67] M.-C. Daniel, D. Astruc, *Chem. Rev.* **2004**, *104*, 293.
[68] X. B. Cao, L. Gu, L. J. Zhuge, W. J. Gao, W. C. Wang, S. F. Wu, *Adv. Funct. Mater.* **2006**, *16*, 896.
[69] H. R. Moon, D.-W. Lim, M. P. Suh, *Chem. Soc. Rev.* **2013**, *42*, 1807.
[70] A. Dhakshinamoorthy, H. Garcia, *Chem. Soc. Rev.* **2012**, *41*, 5262.
[71] T. Ishida, M. Nagaoka, T. Akita, M. Haruta, *Chem. Eur. J.* **2008**, *14*, 8456.
[72] R. Ameloot, M. B. J. Roeffaers, G. De Cremer, F. Vermoortele, J. Hofkens, B. F. Sels, D. E. De Vos, *Adv. Mater.* **2011**, *23*, 1788.
[73] D. Bryce-Smith, A. Harriman, *Photochemistry* **1987**, *18*, 523.
[74] J. de Wild, A. Meijerink, J. K. Rath, W. G. J. H. M. van Sark, R. E. I. Schropp, *Energy Environ. Sci.* **2011**, *4*, 4835.
[75] P. S. Bassi, G. Gurudayal, L. H. Wong, J. Barber, *Phys. Chem. Chem. Phys.* **2014**, *16*, 11834.
[76] Y. Horiuchi, T. Toyao, M. Takeuchi, M. Matsuoka, M. Anpo, *Phys. Chem. Chem. Phys.* **2013**, *15*, 13243.
[77] S. Wang, X. Wang, *Small* **2015**, *11*, 3097 – 3112.
[78] M. Zhao, S. Ou, C.-D. Wu, *Acc. Chem. Res.* **2014**, *47*, 1199.
[79] C. Zou, C.-D. Wu, *Dalton Trans.* **2012**, *41*, 3879.
[80] C. Wang, K. E. deKrafft, W. Lin, *J. Am. Chem. Soc.* **2012**, *134*, 7211 – 7214.
[81] A. Fateeva, P. A. Chater, C. P. Ireland, A. A. Tahir, Y. Z. Khimyak, P. V. Wiper, J. R. Darwent, M. J. Rosseinsky, *Angew. Chem. Int. Ed.* **2012**, *51*, 7440; *Angew. Chem.* **2012**, *124*, 7558.
[82] T. Zhou, Y. Du, A. Borgna, J. Hong, Y. Wang, J. Han, W. Zhang, R. Xu, *Energy Environ. Sci.* **2013**, *6*, 3229.
[83] C. Gomes Silva, I. Luz, F. X. Llabres i Xamena, A. Corma, H. Garcia, *Chem. Eur. J.* **2010**, *16*, 11133.
[84] D. Sun, W. Liu, M. Qiu, Y. Zhang, Z. Li, *Chem. Commun.* **2015**, *51*, 2056.
[85] J. He, J. Wang, Y. Chen, J. Zhang, D. Duan, Y. Wang, Z. Yan, *Chem. Commun.* **2014**, *50*, 7063.
[86] Y.-P. Yuan, L.-S. Yin, S.-W. Cao, G.-S. Xu, C.-H. Li, C. Xue, *Appl. Catal. B* **2015**, *168 – 169*, 572.
[87] T. Toyao, M. Saito, S. Dohshi, K. Mochizuki, M. Iwata, H. Higashimura, Y. Horiuchi, M. Matsuoka, *Chem. Commun.* **2014**, *50*, 6779.
[88] J.-Q. Shen, Y. Zhang, Z.-M. Zhang, Y.-G. Li, Y.-Q. Gao, E.-B. Wang, *Chem. Commun.* **2014**, *50*, 6017.
[89] K. E. deKrafft, C. Wang, W. Lin, *Adv. Mater.* **2012**, *24*, 2014.
[90] J. He, Z. Yan, J. Wang, J. Xie, L. Jiang, Y. Shi, F. Yuan, F. Yu, Y. Sun, *Chem. Commun.* **2013**, *49*, 6761.
[91] R. Lin, L. Shen, Z. Ren, W. Wu, Y. Tan, H. Fu, J. Zhang, L. Wu, *Chem. Commun.* **2014**, *50*, 8533.
[92] Y. Horiuchi, T. Toyao, M. Saito, K. Mochizuki, M. Iwata, H. Higashimura, M. Anpo, M. Matsuoka, *J. Phys. Chem. C* **2012**, *116*, 20848 – 20853.
[93] T. Toyao, M. Saito, Y. Horiuchi, K. Mochizuki, M. Iwata, H. Higashimura, M. Matsuoka, *Catal. Sci. Technol.* **2013**, *3*, 2092.
[94] L. Shen, M. Luo, L. Huang, P. Feng, L. Wu, *Inorg. Chem.* **2015**, *54*, 1191.
[95] M. A. Nasalevich, R. Becker, E. V. Ramos-Fernandez, S. Castellanos, S. L. Veber, M. V. Fedin, F. Kapteijn, J. N. H. Reek, J. I. van der Vlugt, J. Gascon, *Energy Environ. Sci.* **2015**, *8*, 364.
[96] Y. Fu, D. Sun, Y. Chen, R. Huang, Z. Ding, X. Fu, Z. Li, *Angew. Chem. Int. Ed.* **2012**, *51*, 3364; *Angew. Chem.* **2012**, *124*, 3420.
[97] D. Sun, W. Liu, Y. Fu, Z. Fang, F. Sun, X. Fu, Y. Zhang, Z. Li, *Chem. Eur. J.* **2014**, *20*, 4780.
[98] D. Sun, Y. Fu, W. Liu, L. Ye, D. Wang, L. Yang, X. Fu, Z. Li, *Chem. Eur. J.* **2013**, *19*, 14279.
[99] Y. Lee, S. Kim, J. K. Kang, S. M. Cohen, *Chem. Commun.* **2015**, *51*, 5735.
[100] D. Wang, R. Huang, W. Liu, D. Sun, Z. Li, *ACS Catal.* **2014**, *4*, 4254.
[101] Y. Liu, Y. Yang, Q. Sun, Z. Wang, B. Huang, Y. Dai, X. Qin, X. Zhang, *ACS Appl. Mater. Interfaces* **2013**, *5*, 7654 – 7658.
[102] D. Sun, Y. Gao, J. Fu, X. Zeng, Z. Chen, Z. Li, *Chem. Commun.* **2015**, *51*, 2645.
[103] M. B. Chambers, X. Wang, N. Elgrishi, C. H. Hendon, A. Walsh, J. Bonnefoy, J. Canivet, E. A. Quadrelli, D. Farrusseng, C. Mellot-Draznieks, M. Fontecave, *ChemSusChem* **2015**, *8*, 603 – 608.
[104] R. Li, J. Hu, M. Deng, H. Wang, X. Wang, Y. Hu, H.-L. Jiang, J. Jiang, Q. Zhang, Y. Xie, Y. Xiong, *Adv. Mater.* **2014**, *26*, 4783.
[105] S. Wang, X. Wang, *Appl. Catal. B* **2015**, *162*, 494.
[106] S. Wang, J. Lin, X. Wang, *Phys. Chem. Chem. Phys.* **2014**, *16*, 14656.
[107] Q. Liu, Z.-X. Low, L. Li, A. Razmjou, K. Wang, J. Yao, H. Wang, *J. Mater. Chem. A* **2013**, *1*, 11563.
[108] D. Marsh, L. Mink, *J. Chem. Educ.* **1996**, *73*, 1188.
[109] J. H. Cavka, S. Jakobsen, U. Olsbye, N. Guillou, C. Lamberti, S. Bordiga, K. P. Lillerud, *J. Am. Chem. Soc.* **2008**, *130*, 13850.
[110] L. Valenzano, B. Civalleri, S. Chavan, S. Bordiga, M. H. Nilsen, S. Jakobsen, K. P. Lillerud, C. Lamberti, *Chem. Mater.* **2011**, *23*, 1700.
[111] A. Dhakshinamoorthy, A. M. Asiri, H. Garcia, *Chem. Commun.* **2014**, *50*, 12800.
[112] C. G. Silva, A. Corma, H. García, *J. Mater. Chem.* **2010**, *20*, 3141.
[113] T. L. Thompson, J. T. Yates, Jr., *Chem. Rev.* **2006**, *106*, 4428.
[114] N. V. Maksimchuk, K. A. Kovalenko, V. P. Fedin, O. A. Kholdeeva, *Adv. Synth. Catal.* **2010**, *352*, 2943.
[115] M. Alvaro, E. Carbonell, B. Ferrer, F. X. Llabres i Xamena, H. Garcia, *Chem. Eur. J.* **2007**, *13*, 5106.
[116] Q. Li, B. Guo, J. Yu, J. Ran, B. Zhang, H. Yan, J. Gong, *J. Am. Chem. Soc.* **2011**, *133*, 10878.
[117] N. Zhang, Y. Zhang, Y.-J. Xu, *Nanoscale* **2012**, *4*, 5792.
[118] M. Latorre-Sánchez, A. Primo, H. García, *Angew. Chem. Int. Ed.* **2013**, *52*, 11813; *Angew. Chem.* **2013**, *125*, 12029.
[119] S. Linley, Y. Liu, C. J. Ptacek, D. W. Blowes, F. X. Gu, *ACS Appl. Mater. Interfaces* **2014**, *6*, 4658.
[120] T.-F. Yeh, J. Cihlár, C.-Y. Chang, C. Cheng, H. Teng, *Mater. Today* **2013**, *16*, 78.
[121] Q. Xiang, J. Yu, M. Jaroniec, *Chem. Soc. Rev.* **2012**, *41*, 782.
[122] S. Corrent, G. Cosa, J. C. Scaiano, M. S. Galletero, M. Alvaro, H. Garcia, *Chem. Mater.* **2001**, *13*, 715.
[123] B. Ma, F. Wen, H. Jiang, J. Yang, P. Ying, C. Li, *Catal. Lett.* **2010**, *134*, 78.
[124] N. Bao, L. Shen, T. Takata, K. Domen, *Chem. Mater.* **2007**, *19*, 110.
[125] Y. Ma, X. Wang, Y. Jia, X. Chen, H. Han, C. Li, *Chem. Rev.* **2014**, *114*, 9987.
[126] A. Corma, H. Garcia, *J. Catal.* **2013**, *308*, 168.
[127] G. A. Ozin, *Adv. Mater.* **2015**, *27*, 1957.
[128] R. Schlögl, *Angew. Chem. Int. Ed.* **2015**, *54*, 4436; *Angew. Chem.* **2015**, *127*, 4512.
[129] *The Porphyrins: Physical Chemistry, Part A, vol. III* (Ed.: D. Dolphin), Academic Press, New York, **1978**, p. 106.
[130] P. Voyame, K. E. Toghill, M. A. Mendez, H. H. Girault, *Inorg. Chem.* **2013**, *52*, 10949.

[131] A. Dhakshinamoorthy, S. Navalon, A. Corma, H. Garcia, *Energy Environ. Sci.* **2012**, *5*, 9217.
[132] C. Montoro, E. García, S. Calero, M. A. Pérez-Fernández, A. L. López, E. Barea, J. A. R. Navarro, *J. Mater. Chem.* **2012**, *22*, 10155.
[133] S. V. Ley, A. Madin, in *Comprehensive Organic Synthesis* (Eds.: M. T. Barry, F. Ian), Pergamon, Oxford, **1991**, pp. 251 – 289.
[134] S. Higashimoto, N. Kitao, N. Yoshida, T. Sakura, M. Azuma, H. Ohue, Y. Sakata, *J. Catal.* **2009**, *266*, 279.
[135] J. Long, S. Wang, Z. Ding, S. Wang, Y. Zhou, L. Huang, X. Wang, *Chem. Commun.* **2012**, *48*, 11656.
[136] L. Shen, S. Liang, W. Wu, R. Liang, L. Wu, *J. Mater. Chem. A* **2013**, *1*, 11473.
[137] T. W. Goh, C. Xiao, R. V. Maligal-Ganesh, X. Li, W. Huang, *Chem. Eng. Sci.* **2015**, *124*, 45.
[138] L. Chen, Y. Peng, H. Wang, Z. Gu, C. Duan, *Chem. Commun.* **2014**, *50*, 8651.
[139] D. Sun, L. Ye, Z. Li, *Appl. Catal. B* **2015**, *164*, 428.
[140] M. A. Nasalevich, M. G. Goesten, T. J. Savenije, F. Kapteijn, J. Gascon, *Chem. Commun.* **2013**, *49*, 10575.
[141] S. Abedi, A. Morsali, *ACS Catal.* **2014**, *4*, 1398 – 1403.
[142] X. Yu, S. M. Cohen, *Chem. Commun.* **2015**, *51*, 9880 – 9883.
[143] P. Y. Moh, P. Cubillas, M. W. Anderson, M. P. Attfield, *J. Am. Chem. Soc.* **2011**, *133*, 13304.
[144] J. Gascon, M. D. Hernandez-Alonso, A. R. Almeida, G. P. van Klink, F. Kapteijn, G. Mul, *ChemSusChem* **2008**, *1*, 981.
[145] G. J. Lee, D. Kim, M. Lee, *Appl. Opt.* **1995**, *34*, 138.
[146] A. R. Almeida, M. Calatayud, F. Tielens, J. A. Moulijn, G. Mul, *J. Phys. Chem. C* **2011**, *115*, 14164.
[147] S. S.-Y. Cui, S. M.-F. Lo, J. P. H. Charmant, A. G. Orpen, I. D. Williams, *Science* **1999**, *283*, 1148 – 1150.
[148] S. Dai, W. Yan, M. Mahurin, S. H. Overbury, *Chem. Mater.* **2005**, *17*, 1923 – 1925.

Received: June 17, 2015
Revised: August 6, 2015
Published online: March 11, 2016

